PREPARATION AND CHARACTERIZATION OF CERAMIC OXIDE THIN FILMS FOR ELECTRICAL VARISTORS

A DISSERTATION

Submitted in partial fulfillment of the requirements for the award of the degree
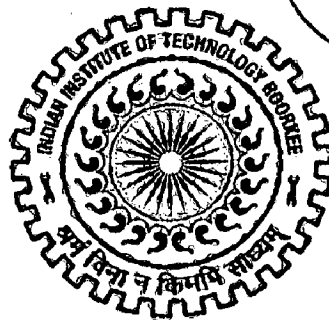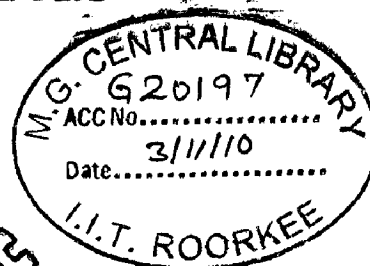
of

MASTER OF TECHNOLOGY

in

METALLURGICAL & MATERIALS ENGINEERING
(With Specialization in Industrial Metallurgy)

By

NIRANJANA A.P

DEPARTMENT OF METALLURGICAL & MATERIALS ENGINEERING
INDIAN INSTITUTE OF TECHNOLOGY ROORKEE
ROORKEE - 247 667 (INDIA)
JUNE, 2010

CANDIDATE'S DECLARATION

I hereby declare that the proposed work presented in this dissertation titled **"Preparation and Characterization of Ceramic Oxide Thin Films for Electrical Varistors "** in partial fulfillment of the requirements for the award of the degree of **Master of Technology** with the specialization in **Industrial Metallurgy,** submitted in the **Department of Metallurgical and Materials Engineering, Indian Institute of Technology Roorkee, Roorkee, India,** is an authentic record of my own work carried out during the period from June 2009 to June 2010 under the supervision of **Dr. Anjan Sil,** Professor, Department of Metallurgical and Materials Engineering, Indian Institute of Technology Roorkee, Roorkee, India.

I have not submitted the matter embodied in this dissertation for the award of any other degree.

Date: 30·06·10

Place: Roorkee

(NIRANJANA A. P)

CERTIFICATE

This is to certify that the above declaration made by Mr. Niranjana A.P is correct to the best of my knowledge and belief.

Dr. Anjan Sil 18/6/10

Professor,

Department of Metallurgical and Materials Engineering,

Indian Institute of Technology Roorkee,

Roorkee- 247667 (INDIA)

ACKNOWLEDGMENT

I am highly indebted to **Dr. Anjan Sil**, Professor, Department of Metallurgical and Materials Engineering, Indian Institute of Technology, Roorkee, for encouraging me to undertake this dissertation as well as providing me all the necessary guidance and inspirational support throughout this dissertation work. He has displayed unique tolerance and understanding at every step of progress. It is my proud privilege to have carried out this dissertation work under his able guidance.

It is my pleasure to express my sincere gratitude to Dr. P. K. Ghosh, Prof. and Head, Department of Metallurgical and Materials Engineering, Indian Institute of Technology, Roorkee, for his inspiration and co-operation at every stage of this work.

I am very thankful to Dr. Anil Kumar, Prof. and Head, Centre of Nanotechnology, Indian Institute of Technology, Roorkee, for the support extended to me for carrying out the spin coating.

I would like to thank all the faculty members and Laboratory superintendents, Department of Metallurgical and Materials Engineering, Indian Institute of Technology, Roorkee, where I have learnt so much, within the scope of the project and without whose support, the project could never have been completed. Whether it was monetary, authoritative or technical support, they always stood by, and I am deeply indebted to them.

I am equally thankful to Dr. Kevin M. Knowles, Senior Lecturer, Department of Materials Science & Metallurgy, University of Cambridge for his time to see our experiment, enlightening discussion and sincere suggestions.

A sincere thanks to the staff of the Institute Instrumentation Center, Indian Institute of Technology, Roorkee, who worked hard and long to provide with the characterization of samples through the plethora of cases they had to handle.

I would also like to extend my gratitude to Dr. Gurpreet Singh, Dr.Kuldeep Rana, and research scholars of Department of Metallurgical and Materials Engineering, Indian Institute of

ABSTRACT

The composition, microstructure and electrical properties of ZnO based ceramic films (ZnO-V_2O_5-MnO) have been analysed. Samples were prepared by novel sol-gel process with ZnO-0.5 mol% V_2O_5-x mol% MnO (x = 0.5, 1.0, 1.5) compositions. ZnO based ceramic films, with a thickness of 0.25-3 μm, were deposited on ordinary glass and ITO coated glass substrate by spin coating method. The precursors were prepared initially by dispersing doped-ZnO ceramic nano-powders into the sols, prepared by dissolving zinc acetate into 2-methoxyethanol and stabilized by ethanolamine and acetic acid glacial and doped with amonium metavanadate and manganese acetate. The doped-ZnO ceramic nano-powders were prepared by sol-gel processing through dried and calcined at 150°C and 800°C respectively. The films were prepared by the spin coating method with the substrate spinning rate between 2000 and 3000 rpm. After each deposition, the films were heat treated at 240°C for 10 min. After 10 to 30 layers of the film deposition on ordinary glass and ITO coated glass, the films were annealed for 60 min at 550°C and 700°C respectively. The films have been characterized by X-ray diffraction for phase determination and field emission scanning electron microscopy (FESEM) for grain structure observation. The nonlinear V-I characteristics of the films for use as varistors were studied using KEITHLEY 2400 source meter. All the microstructures consisted of ZnO grains with zinc vanadate and zinc manganate compounds as minority secondary phases. The secondary phases $Zn_3(VO_4)_2$ and $Zn_4V_2O_9$ were found in the samples annealed at 700°C. FESEM micrographs show that the film prepared is uniform and the grain sizes are in the range of 25-40 nm and 70-90 nm for doped ZnO films annealed at 550°C and 700°C respectively. All the samples exhibited nonlinear current-voltage behavior, with nonlinear coefficient, α, ranging between 103 and 420. The highest values of α is achieved for the films annealed at 700°C and having composition of ZnO-0.5 mol% V_2O_5-1.5 mol% MnO with a thickness of 3μm.

CONTENTS

LIST OF FIGURES

LIST OF TABLES

1. INTRODUCTION

Ceramics are materials that are composed of inorganic substances (usually a combination of metallic and nonmetallic elements).

Ceramics offer many advantages compared to other materials. They are harder and stiffer than steel, more heat and corrosion resistant than metals or polymers, less dense than most of the metals and their alloys, and the raw materials are inexpensive and available in plenty. Ceramics display a wide range of properties which facilitate their use in many different product areas.

Ceramics have characteristics that enable them to be used in a wide variety of applications including:

1. High heat capacity and low heat conductance.
2. Corrosion resistance.
3. Electrically insulating, semiconducting, or superconducting.
4. Nonmagnetic and magnetic.
5. Hard and strong, but brittle.

Some ceramics are semiconductors. Most of these are transition metal oxides that are II-VI semiconductors, such as zinc oxide (ZnO).

ZnO is an n-type semiconductor with unique properties such as high infrared reflectivity, acoustic characteristics, high electrochemical stability, transparency and excellent electronic properties. ZnO is inexpensive, relatively abundant, chemically stable, easy to prepare and non-toxic. Most of the doping materials that are used with ZnO are also readily available.

In addition to cost savings, ZnO offers the following properties.

- High carrier mobility
- Wide band gap (3.37 eV)
- Low temperature process

1

Numerous electrically conductive oxides have been discovered and extensively investigated. Of these, zinc oxide (ZnO) is well known for its transparency when made into thin films and is expected to find wide use as transparent electrodes for many devices, such as electro chromic displays (ECDs), electroluminescent displays, liquid crystal displays (LCDs) and solar cells. ZnO thin films with suitable dopants are also used as photoconductors in electrography, varistors and sensor elements in sensing combustible gases. One of the most widely used of these is the varistor.

Varistors are the devices that exhibit the property that resistance drops sharply at a certain threshold voltage. Once the voltage across the device reaches the threshold, there is a breakdown of the electrical structure in the vicinity of the grain boundaries, which results in its electrical resistance dropping from several mega ohms down to a few ohms.[1] The major advantage of these is that they can dissipate a lot of energy, and they self reset after the voltage across the device drops below the threshold, its resistance returns to being high.

This non-ohmicity of voltage—current properties is due to the presence of a double Schottky barrier formed at active grain boundaries containing many trap states. Various doping systems used for the purpose of creating the Schottky junction are bismuth, yttrium, praseodymium, cobalt, antimony, manganese etc.[2]

Owing to highly nonohmic properties, these ceramic devices are used widely in the field of overvoltage protection systems from electronic circuits to electric power systems. The best demonstration of their ability can be found in electrical substations, where they are employed to protect the infrastructure from lightning strike. They have rapid response, low maintenance requirement, and do not appreciably degrade from use, making them virtually ideal devices for this application. A typical bulk varistor is shown in Fig. 1.1.
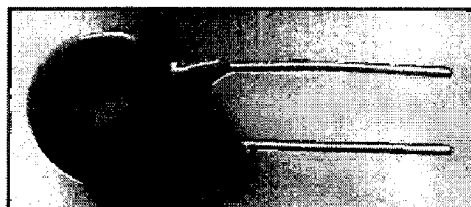
Fig.1.1. A typical bulk varistor.

As the development of large scale integration (LSI) and very large-scale integration (VLSI) electronics is in steep progress, transient surge suppression for low-voltage electronic circuits has attracted attention and varistors with highly nonlinear V-I characteristics at low voltages are necessary as protective devices. Developing materials that exhibit high nonlinear current-voltage characteristics at lower voltage has become an important aspect in the academic and industry researches of the varistor. There are two approaches for lowering breakdown voltage for device. One is to make a disk thinner. The other is to lower the breakdown voltage per unit thickness.

Sol-gel processing has proved to be a much easier and more cost effective processing technique. Process variations include dip-coating, drop-coating, spin coating etc. Spin coating is a fairly new process in which solution is dispensed on the substrate rotating at a speed of around 2000-3000 rpm. The deposited film is cured at elevated temperature and recoating is done and the final film is calcined at suitable temperature for sufficient period.

The objective of the present study is to investigate the possibility of developing good quality zinc oxide-based ceramic thin films which can be used as varistor devices to protect electronic circuits from voltage surges. Manganese and Vanadium doped ZnO based ceramic thin films were deposited using sol-gel process and spin coating technique. Characterizations of the film were done by using X-ray diffraction (XRD) and Field emission scanning electron microscopy (FESEM). The electrical properties of the films were discussed on the basis of the measurements of V-I characteristics.

2. LITERATURE REVIEW

Despite of its benefits, one of the few drawbacks of semiconductor technology is the vulnerability of solid-state devices to over-voltages. Even voltage pulses of very low energy can produce interference and damage, sometimes with far-reaching consequences. So, as electronics make its way into more and more applications, optimum overvoltage or transient suppression becomes a design factor of decisive importance.

Varistors have proven to be excellent protective devices because of their application flexibility and high reliability. The metal oxide varistor, with its extremely attractive performance/price ratio, is an ideal component for limiting surge voltage and current as well as for absorbing energy.

2.1 Varistors

Varistors (Variable Resistors) are voltage-dependent resistors with a symmetrical *V-I* characteristics curve (Fig. 2.1) whose resistance decreases with increasing voltage. Connected in parallel with the electronic device or circuit that is to be guarded, they form a low-resistance shunt when voltage increases and thus prevent any further rise in the overvoltage.
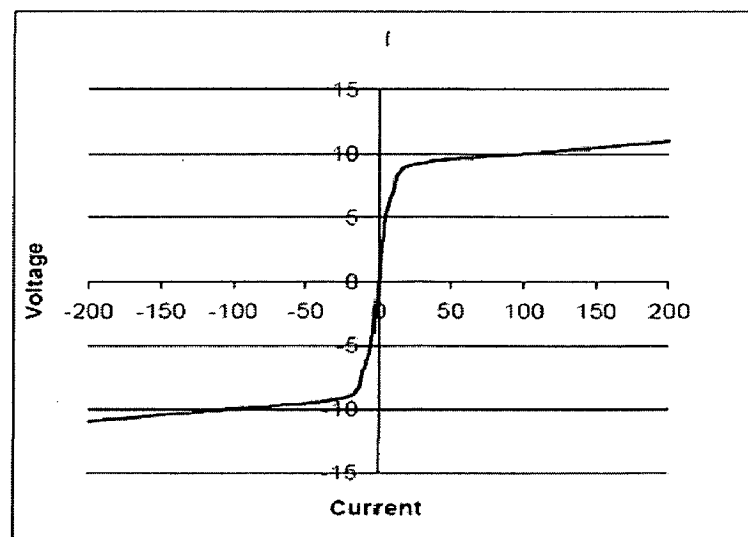
Fig. 2.1. Typical *V-I* characteristics of a metal oxide varistor on a linear scale.

The degree of non-ohmic property is usually expressed by a non-ohmic exponent, α, defined by the following equation:

$$I = (V/C)^{\alpha} \qquad \text{---------- (2.1)}$$

where, C is a constant and α is termed as non linear exponent. By studying the *V-I* characteristics, the value of α can be estimated. [1][3]

2.1.1 V-I Characteristics of varistor
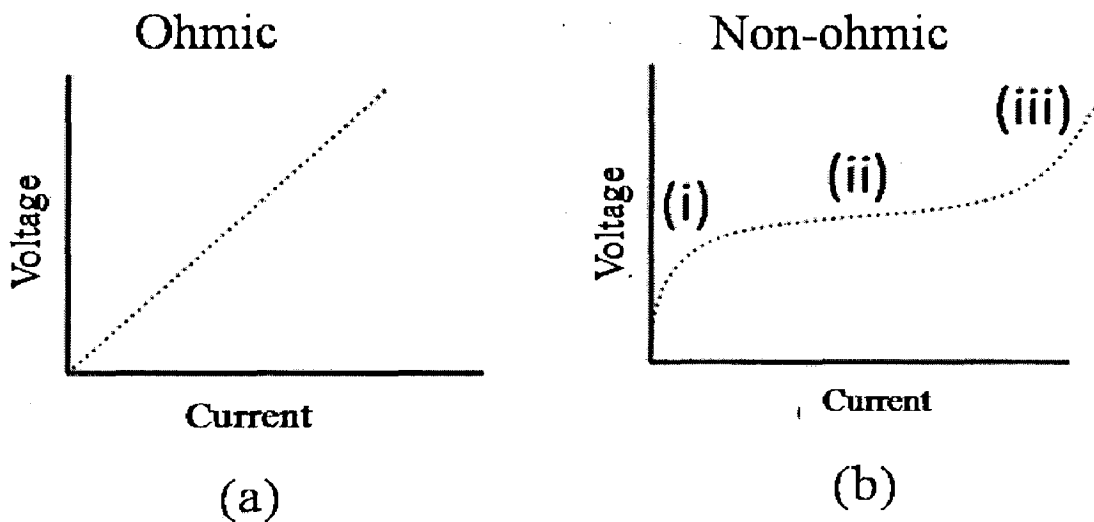
Fig. 2.2. General V-I characteristics of (a) ohmic materials and (b) non-ohmic materials.

Figure 2.2 shows the ohmic and non-ohmic behaviour of materials. The ohmic behaviour simply explains that the material follows ohm's law for entire voltage range applied. The curve is a simple straight line with a slope equal to constant resistance of the material. The V-I curve of a non-ohmic material consists of three regions:

1. An ohmic region at low voltage.
2. A non-ohmic region having high α-value at intermediate voltage.
3. A non-ohmic region having a low α-value at high voltage.

It is also reported that the non-ohmic region becomes narrow when the temperature is increased.[1] Matsuoka proposed a model to calculate the resistivity of the segregation layer, in which each of ZnO grains is surrounded by a segregation layer and observed that the ZnO grains

5

as the region of high conductivity and oxide segregation layer as the region of high resistivity.[1] The model was derived assuming a composite structure, just like the layering of bricks in a wall. In recent studies also, the brick layer model has been used to estimate the resistivity of the grain boundary phases.

Mason et al. even derived a model for the nano-regime of grains and their boundaries.[4] When the voltage applied is below the threshold, the electrons cannot cross the highly resistive segregation layer and only the leakage current flows. As soon as the voltage is increased above threshold, the electric field at the segregation layer increases to a very high extent, and an avalanche of electrons crosses the boundary. This causes the non-ohmic behaviour to be observed. From the slope of V-I curve in the non-linear region, the value of non-linear exponent, α, can be calculated as below:

$$\alpha = \frac{dI/I}{dV/V} = \frac{\log_{10} I_2 - \log_{10} I_1}{\log_{10} V_2 - \log_{10} V_1} \quad \text{---------} (2.2)$$

where V_1 and V_2 are the voltages at the currents of I_1 and I_2 respectively.

From the symmetrical brick layer model, one can understand that the reverse current or so called leakage current plays most important role in the voltage-current behaviour of these materials. If one follows the diffusion theory, then the reverse current would have only a small dependence on the applied voltage. Therefore, it is unlikely that the diffusion theory can be applied to understand the non-linear behaviour of these ceramics. However, this non-linearity can be attributed to tunnelling of electrons and avalanche breakdown. It has been shown long back by the researchers that the mechanism based on tunnelling requires the segregation layer to be of less than 100 Å. The avalanche breakdown theory needs a high electric field of about 10^6 V/cm applied to the segregation layer.

Another theory, which is most commonly used to describe non-linearity, is based on space charge limited current. This behaviour with trap levels present lowers the electric field required for the electrons to tunnel across the grain boundaries. Many different oxide phases which remain present at the segregation layer cause the creation of trap levels. On the basis of Lambert's space charge limited current theory also, the value of non-linear exponent α can be calculated which is found to be in good agreement with the observed value.[1]

ZnO varistors are polycrystalline materials composed of semiconducting ZnO grains with their attendant grain boundaries. The resistivity of a ZnO grain is 0.1-1 Ω-cm. The grain boundaries are highly resistive and show non-ohmic property. The breakdown voltage per grain boundary is about 3 V. The breakdown voltage of the sintered body is proportional to the number of grain boundaries between the two electrodes. This indicates that the breakdown voltage is proportional to the inverse of the ZnO grain size. The sizes of ZnO grains in bulk varistor samples are usually 5-20 μm and depend on the material composition, sintering temperature and time.[5]

2.1.2 Microstructure and conduction mechanism of varistor

Sintering zinc oxide with other metal oxide additives under specific conditions produces a polycrystalline ceramic whose resistance exhibits a pronounced dependence on voltage. This phenomenon is called the varistor effect.

Fig. 2.3 shows the conduction mechanism in a varistor element in simplified form. The zinc oxide grains are highly conductive, while the intergranular boundary formed of other oxides is highly resistive. Only at those points where zinc oxide grains meet during sintering produce "microvaristors", comparable to symmetrical zener diodes (protection level approx. 3.5 V). The electrical behavior of the metal oxide varistor, as indicated in Fig. 2.3, results from the number of microvaristors connected in series or in parallel.

This implies that the electrical properties are controlled by the physical dimensions of the varistor:

1. Twice the ceramic thickness produces twice the protection level because then twice as many microvaristors are arranged in series.

2. Twice the area produces twice the current handling capability because then twice the number of current paths is arranged in parallel.

3. Twice the volume produces almost twice the energy absorption capability because then there are twice as many absorbers in the form of zinc oxide grains.
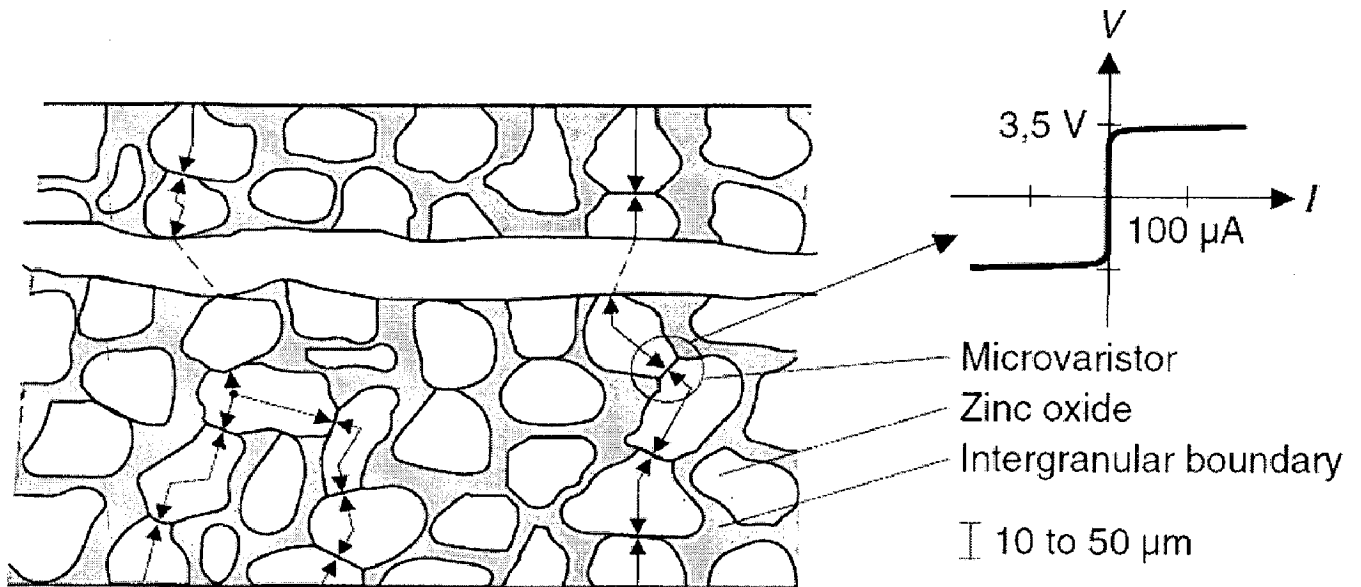
Fig.2.3. Conduction mechanisms in a varistor material.

The series and parallel connection of the individual microvaristors in the sintered body of a MOV also explains its high electrical load capacity compared to semiconductors. While the power in semiconductors is dissipated almost entirely in the thin p-n junction area, in a MOV it is distributed over all the microvaristors, i.e., uniformly throughout the components volume. Each microvaristor is provided with energy absorbers in the form of zinc oxide grains with optimum thermal contact. This permits high absorption of energy and thus exceptionally high surge current handling capability.

A typical ZnO based varistor is a very complex chemical system that contains several dopants, such as Bi_2O_3, CoO, MnO, Sb_2O_3, and Cr_2O_3. It has been proposed that the dopants responsible for the formation of the varistor behaviour are cations of large ionic radii, with low solubility in ZnO at low temperature, like Bi, Pr, Ba, Sr, or Ca.[6-9] These dopants are often called "varistor formers". The other dopants are added for improving the nonohmic properties, such as CoO and MnO, or the densification of ceramics and their reliability, such as Sb_2O_3 and Cr_2O_3. Several studies have been done to investigate the role of the various additives on the microstructure development and electrical properties of ZnO varistors.[7-10]

2.1.3 Role of Mn and V doping on ZnO varistor

1. The addition of small amounts of vanadium and manganese oxides together to zinc oxide can produce good varistor behaviour with non-linear coefficients, α.[11-14]

2. The addition of MnO to the $ZnO-V_2O_5$-based ceramics was found to reduce abnormal grain growth of ZnO. The varistor properties were improved with the increase of MnO concentration.[6,15-16]

3. V_2O_5 is also a better sintering aid compared to Bi_2O_3 since it has been found that V_2O_5-doped ZnO materials can be densified to the same level at a lower temperature compared to Bi_2O_3-doped ZnO materials.[17-18]

2.2 Film preparation

ZnO thin films are prepared by many methods, including chemical vapor deposition (CVD), magnetron sputtering, molecular beam epitaxy (MBE), pulsed laser deposition (PLD), spray pyrolysis, and the sol–gel technique.[19] The properties of ZnO thin films are closely related to their microstructures which depend greatly on the preparation methods and conditions.

However, among all of these techniques, the sol–gel process is particularly attractive because this technique offers good homogeneity, ease of composition control, low processing temperature, large area coatings, low equipment cost and good optical properties. Particularly, the sol–gel processes are efficient in producing thin, transparent, multi-component oxide layers of many compositions on various substrates, including glass.[20-23]

2.2.1 Sol-gel process

The principal advantages of sol-gel processing include the ability to achieve oxygen and ionic stoichiometry during the formation reaction, to synthesize complex composition single phase materials, to form higher purity products through the use of high purity reagents, and to provide coatings over complex geometries including the insides of tubes. However, these advantages are to put in balance with the raw materials high cost, the long processing time involved, the non-uniformity of the films, and the formation of cracks upon drying.[24]

Sol-gel involves a four stage process: dispersion, gelation, drying, and firing. A stable liquid dispersion or *sol* of the colloidal ceramic precursor is initially formed in a solvent with appropriate additives. By changing the concentration (aging) or pH, the dispersion is "polymerized" to form a solid dispersion or *gel*. The excess liquid is removed from this gel by drying and the final ceramic is formed by firing the gel at higher temperatures.

The sol-gel process is a versatile solution process for making ceramic and glass materials. In general, the sol-gel process involves the transition of a system from a liquid "sol" (mostly colloidal) into a solid "gel" phase. Applying the sol-gel process, it is possible to fabricate ceramic or glass materials in a wide variety of forms: ultra-fine or spherical shaped powders, thin film coatings, ceramic fibers, micro porous inorganic membranes, monolithic ceramics and glasses, or extremely porous aerogel materials. An overview of the sol-gel process is presented in a simple graphic work below.
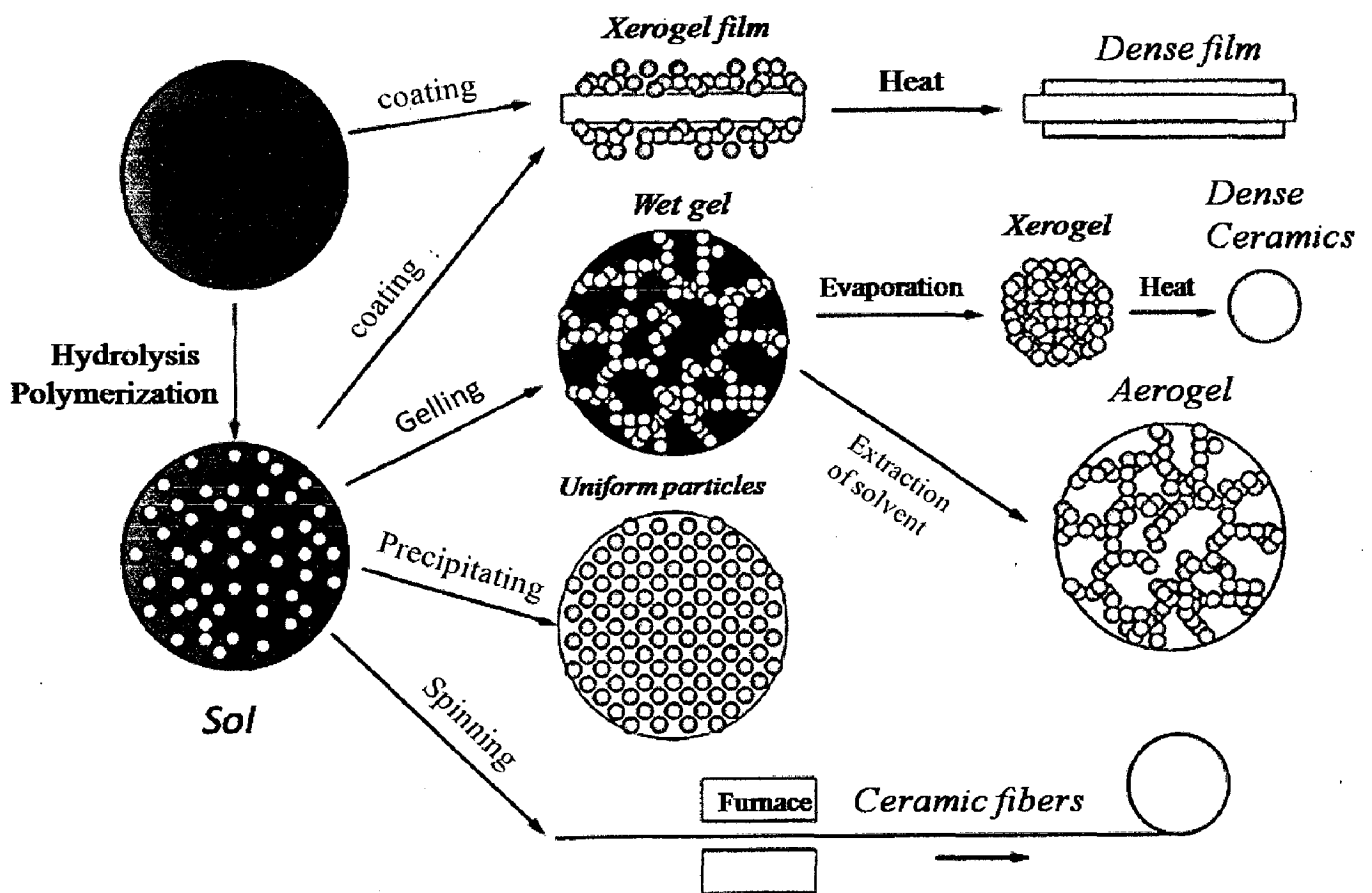

Fig.2.4. Sol-gel method and the product development using this method.

As its name indicates, the principle of the sol-gel technique consists of converting the sol which is a suspension of colloidal or polymeric particles in a solvent, into a semisolid phase known as gel. Commonly, the most preferred starting reagents are metal alkoxides, with general formula:
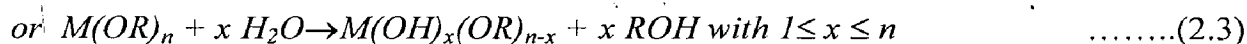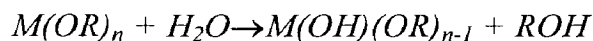
M(OR)n

where M = metal

R = alkyl group such as methyl (CH₃), ethyl (C₂H₅), propyl (C₃H₇)

or butyl (C₄H₉)

n = the valence of the metal atom.

The transition from sol to gel involves two key steps, hydrolysis and condensation.[24-25] Hydrolysis occurs by introducing water in the sol. In this process, the alkoxide groups (OR) are replaced stepwise by hydroxyl groups (OH) as summarized below.

$$M(OR)_n + H_2O \rightarrow M(OH)(OR)_{n-1} + ROH$$

$$or\ M(OR)_n + x\ H_2O \rightarrow M(OH)_x(OR)_{n-x} + x\ ROH\ with\ 1 \leq x \leq n \qquad ....(2.3)$$

Once partially or totally hydrolyzed, the metal hydroxides undergo a stepwise polycondensation which is summarized as follows:

$$2M(OR)_nOH \rightarrow H_2O + {}_n(OR)\ M\text{-}O\text{-}M\ (OR)_n \qquad ....(2.4)$$
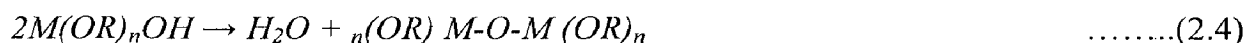
The condensation reaction involves hydroxyl groups and results in M-O-M linkages which, in turn, yields a three dimensional network (called gel) upon a polymeric weight and cross linking-degree increase. The gel state is then best described as a viscoelastic material composed of interpenetrating solid and liquid phases.[26] Its structure is strongly dependent on the water content in the system and whether acid or base was used as hydrolysis catalyser.

However, the gel itself is not an end product. To obtain coatings, ceramic powders or monolithic shapes, the amorphous gel must be dried and crystallized at high temperatures. Most difficulties arise during the drying stage and are mainly caused by the removal of large amounts of solvent trapped in the polymeric network. Indeed, the gel is prone to shrink by a large amount and

capillary forces induce the formation of cracks. To minimize these effects, gels are normally dried by slow evaporation and for coatings, the thickness usually must not exceed 10 µm.

The oldest commercial exploitation of the sol-gel technique, deals with the preparation of coatings. Industrial applications include the development of thin films with specific mechanical, optical or electrical properties, as well as chemical or physical protective properties. There exist at least three coating methods, which are: dip-coating, spin-coating and spray-coating.

2.2.2 Spin coating

Spin coating has been used for several decades for the application of thin films. A typical process involves depositing a drop of a fluid onto the center of a substrate and then spinning the substrate at high speed (typically around 3000 rpm). The physics behind spin coating involves a balance between centrifugal forces controlled by spin speed and viscous forces which are determined by solvent viscosity.
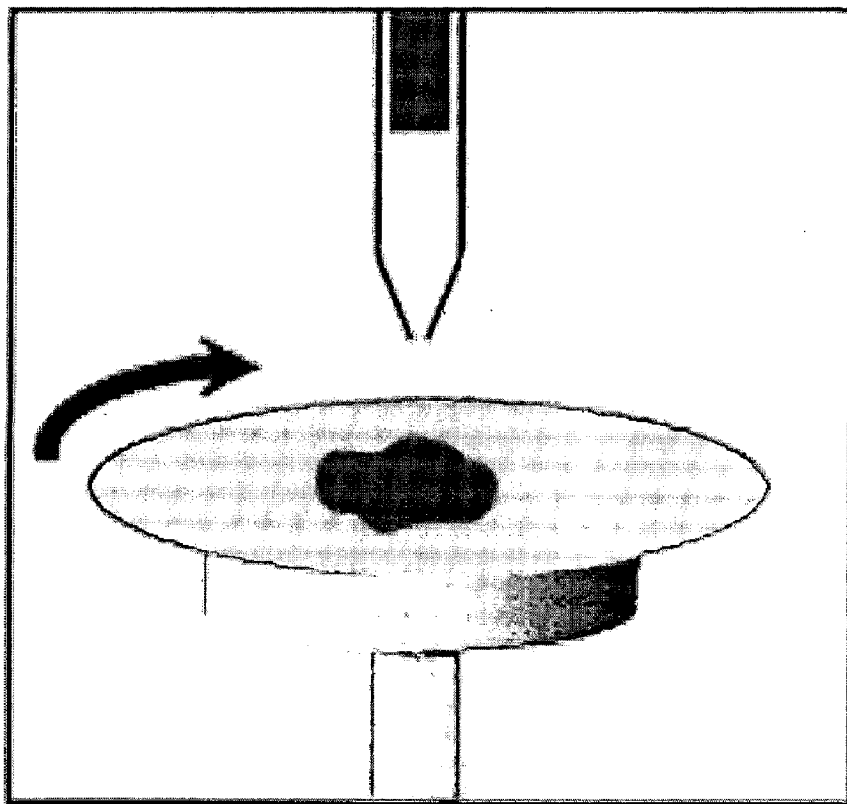

Fig. 2.5. Fluid drop on substrate.

2.2.2.1 Stages of Spin Coating Technique

Although different engineers count things differently, there are four distinct stages to the spin coating process.[27-28]

1. Deposition of the coating fluid onto the wafer or substrate. This can be done by using a nozzle and pouring the coating solution or by spraying it onto the surface. A substantial excess of coating solution is usually applied compared to the amount that is required.
2. Acceleration of the substrate up to its final, desired, rotation speed.
3. Spinning of the substrate at a constant rate; fluid viscous forces dominate the fluid thinning behavior.
4. Spinning of the substrate at a constant rate; solvent evaporation dominates the coating thinning behavior.
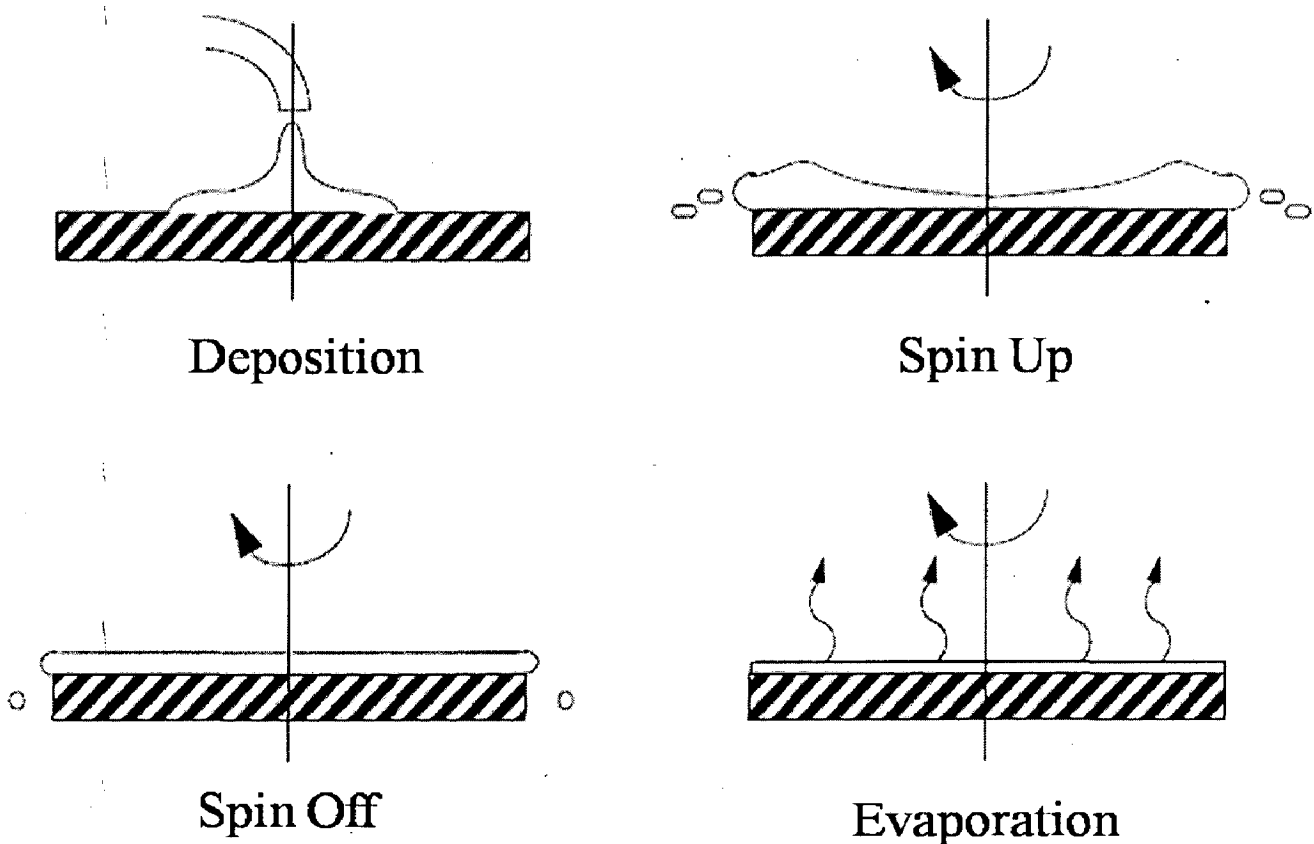
Deposition

Spin Up

Spin Off

Evaporation

Fig. 2.6. The four stages of spin coating process.

4. EXPERIMENTAL PROCEDURE

3.1 Sol preparation

ZnO based films were prepared in the following way:

The flowchart that shows the procedure used for preparing ZnO-based ceramic films is given in Fig. 3.1. The precursors were fabricated by dispersing the doped-ZnO composite nano-powders into the sol. The sol was prepared by zinc acetate dehydrate ($Zn(CH_3COO)_2 \cdot 2H_2O$, M.W-219.49), dopants such as Amonium metavanadate (NH_4VO_3, M.W-117) and Manganese acetate GR (tetrahydrate), [$C_4H_6MnO_4 \cdot 4H_2O$, M.W-245.09] and the solvents, such as 2-methoxyethanol [$C_3H_8O_2$, M.W-76.10]. First the zinc acetate solution is prepared by dissolving zinc acetate dihydrate in 2-methoxyethanol with the addition of ethanolmine (MEA) ($H_2NCH_2CH_2OH$, M.W-61.08) at 60-80°C and then the dopant solution prepared in the ᶜ· ᵒne way by dissolving the dopants in 2-methoxyethanol by the addition of ethanolamine (MEA) and acetic acid glacial (CH_3COOH, M.W-60.05) at 60–80°C. The molar ratio of MEA to zinc acetate was maintained at 1.0 and the concentration of zinc acetate was 0.5-0.9 mol l^{-1}. The dopant solution was added to the zinc acetate solution in such a way that the final composition in mol% of ZnO, V_2O_5 and MnO was in the relative ratio of 98:0.5:1.5. The resultant solution is stirred at room temperature for more than 24 h to yield a clear, stable and homogeneous sol. This sol was then divided into two parts. One part was first dried at 150°C and then calcined at 800°C in air to produce doped-ZnO composite nano-powder. This powder was then dispersed throughout into another part of the sol at the ratio of powder to sol of 5–10 gm per 100 ml to produce the precursor solution. In other method, the sol without powder dispersion is used to develop films. Both the methods of film preparation yielded the same results and latter method is advantageous in terms of time and energy saving. So sol without powder dispersion method of film preparation is adopted for further studies. The colour of sol which changes with additives is shown in Fig. 3.2 and magnetic stirrer used for sol preparation is shown in Fig. 3.3.
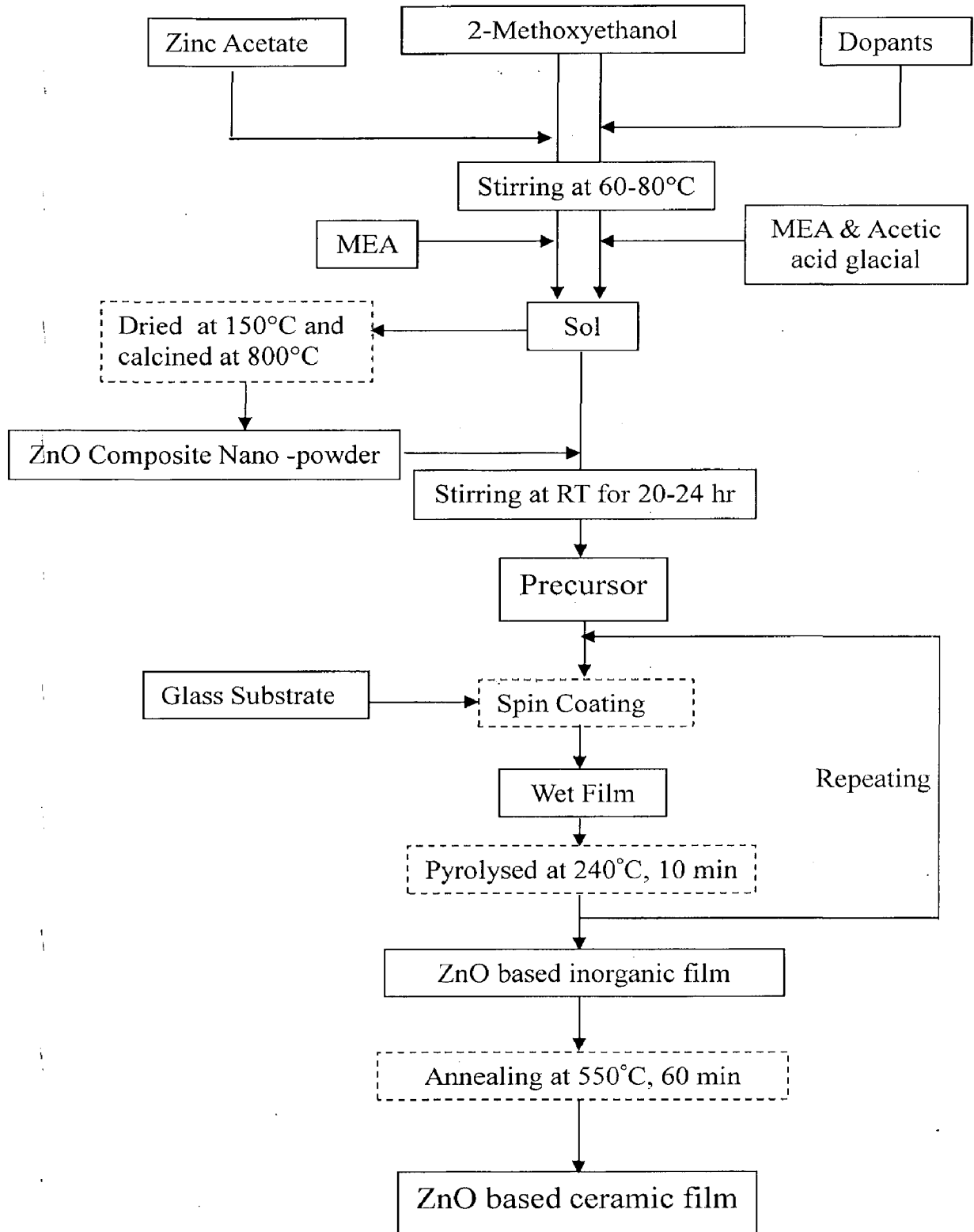
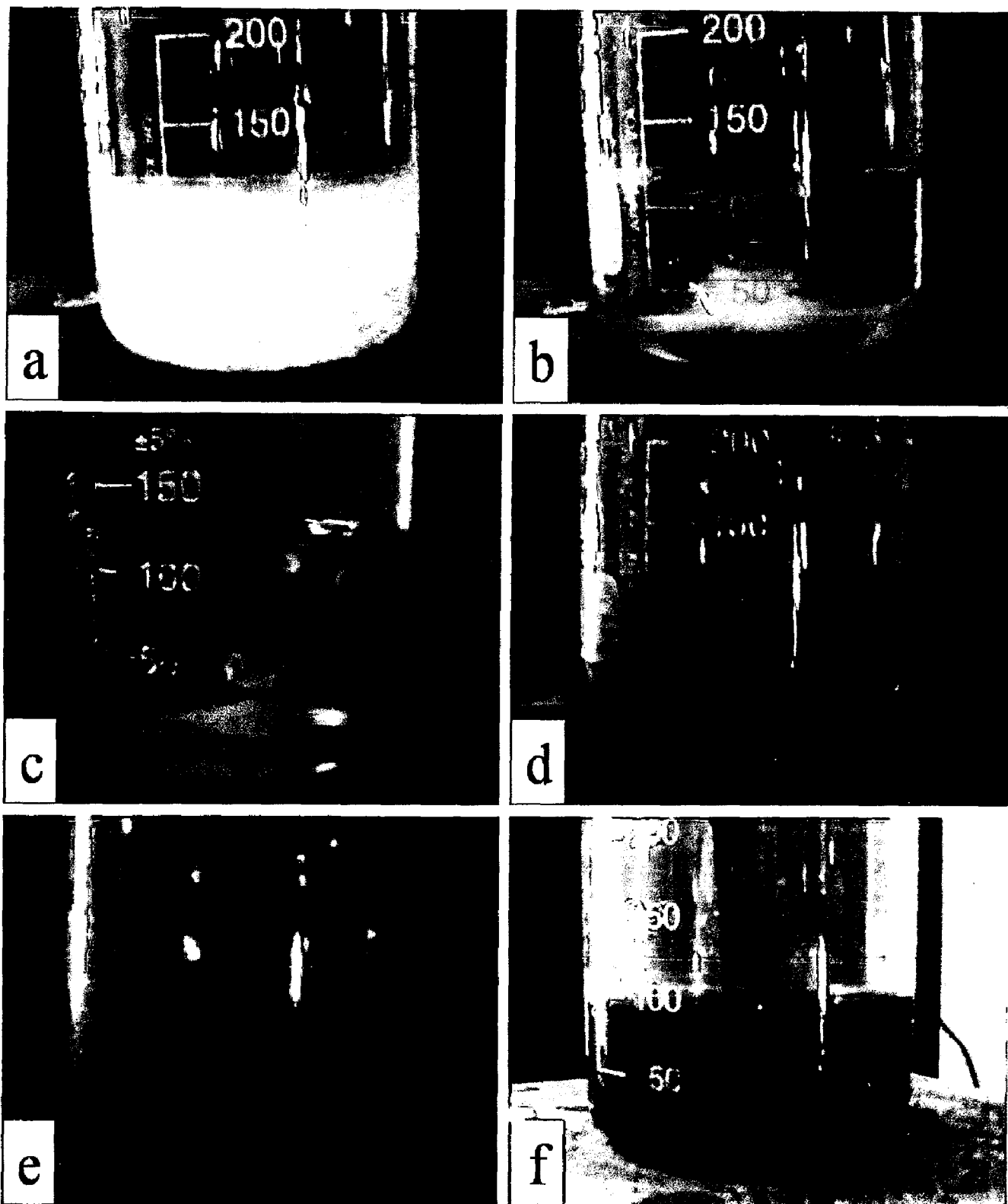Fig. 3.1. Flowchart showing the procedure for preparing ZnO based ceramic films.

Fig. 3.2. Change in colour of sol with additives, (a) Zn acetate in 2-methoxyethanol, (b & c) Clear solution of sol during addition of MEA, (d) After complete addition of MEA, (e) After addition of dopants and acetic acid glacial and (f) Sol after stirring for 24 hrs.
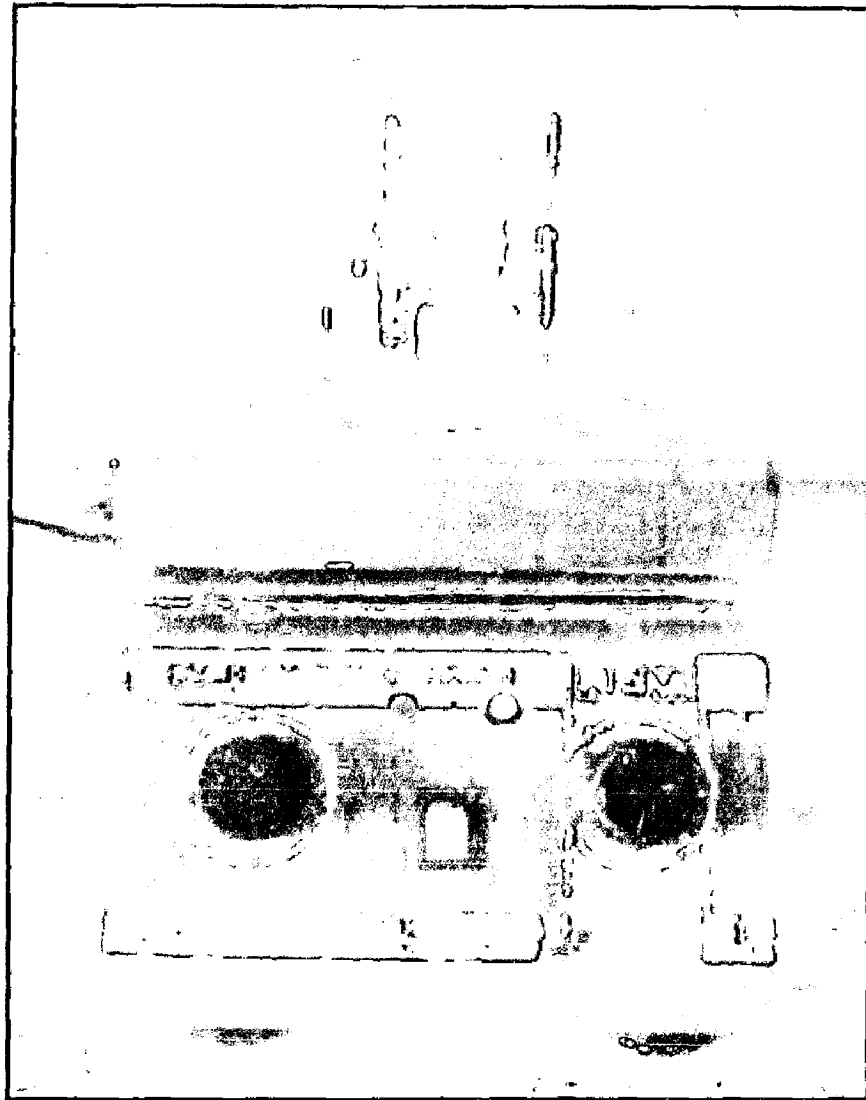
Fig. 3.3. Clear solution while stirring using magnetic stirrer.

3.2 Film preparation

ZnO based ceramic thin films were deposited using spin coating technique. The spin coater used for film preparation is shown in Fig. 3.4. The films were prepared on the ordinary glass / ITO coated glass substrates by repeated spin coating at room temperature, with the substrate spinning rates of 2000–3000 rpm with the spinning time varying between 30 s and 210 s. After each deposition, the films were heated in air oven at 240°C for 10 min. The deposited films on normal glass were annealed in muffle furnace at 550°C for 30/60 min and furnace cooled. Another set of

the films on ITO coated glass substrate were annealed at 700°C for 60 min and furnace cooled. Samples prepared with different process parameters are given in Table 3.1.
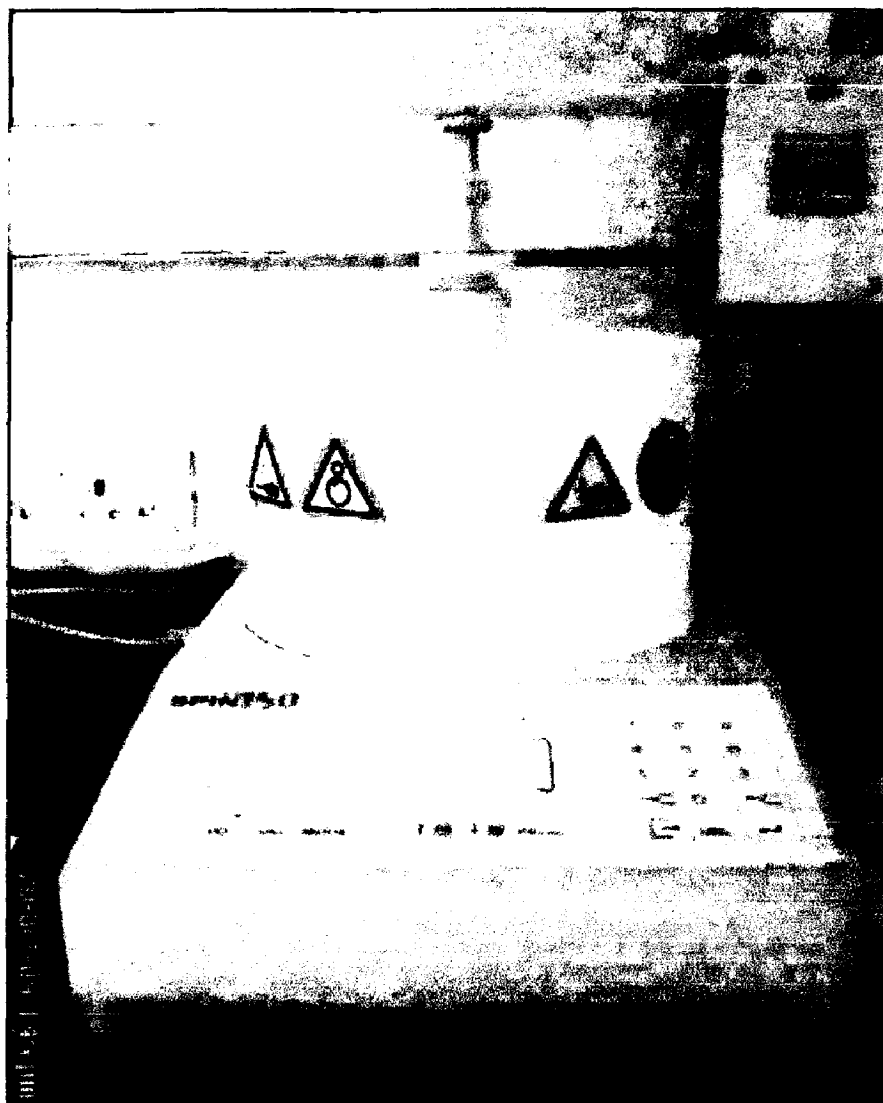

Fig. 3.4. Spin coater used for the film depositions.

Table 3.1. The different parameters used in ZnO based films preparations.

Sample identification	Composition (mole %) ZnO:V$_2$O$_5$:MnO	Sol conc. (mol l^{-1})	Spin speed (rpm)	Spinning time (secs)	Pre-heating temp. (°C)	Soaking time (min)	No. of layers	Annealing temp. (°C)	Soaking time (min)
ZV - Pd	99.5:0.5:0.0	0.5	-	-	150	60	-	820	60
ZV - Pdf	99.5:0.5:0.0	0.5	3000	210 (1 drop/10sec)	80	30	02	550	30
ZV - 1	99.5:0.5:0.0	0.5	3000	-do-	80	30	01	550	30
ZV - 2	99.5:0.5:0.0	0.5	3000	-do-	80	30	02	550	30
ZV - 3	99.5:0.5:0.0	0.5	3000	-do-	80	30	03	550	30
ZV 0.5M- Pd	99.0:0.5:0.5	0.9	-	-	150	60	-	820	60
ZV 0.5M - 1	99.0:0.5:0.5	0.9	3000	210 (1 drop/10sec)	-	-	06	550	30
ZV 1.0M - 1	98.5:0.5:1.0	0.9	2500	15 (cont. drops)	350	30	06	350	30
ZV 1.0M - 2	98.5:0.5:1.0	0.9	2500	-do-	350	30	06	550	30
ZV 1.0M - 3	98.5:0.5:1.0	0.9	2500	20 (cont. drops)	-	-	17	550	30
ZV 1.0M - 4	98.5:0.5:1.0	0.9	2500	-do-	-	-	17	550	60-90
ZV 1.5M - 1	98.0:0.5:1.5	0.9	3000	210 (1 drop/10sec)	450	30	06	550	30
ZV 1.5M - 2	98.0:0.5:1.5	0.9	3000	30 (1 drop/5sec)	240	10	15	550	60
ZV 1.5M - 3	98.0:0.5:1.5	0.9	3000	-do-	240	10	15	550	120
ZV 1.5M - 4	98.0:0.5:1.5	0.9	3000	-do-	240	10	15	550	180
ZV 1.5M - 5	98.0:0.5:1.5	0.9	3000	60 (1 drop/5sec)	240	10	30	550	60
ZV 1.5M - 6	98.0:0.5:1.5	0.9	3000	-do-	240	10	30	700	60
Z-1	100% ZnO	0.9	3000	30 (1 drop/5sec)	240	10	12	550	60
Z-2	100% ZnO	0.9	3000	-do-	240	10	12	700	60

3.3 Film characterization

3.3.1 X-ray diffraction

The crystalline phases in the films were studied by X-ray diffraction (XRD). The X-ray diffraction experiments were performed on a BRUKER D8 X-Ray Automatic Diffractometer. The X-ray diffractometer was set to 40 kV and 30 mA current, utilizing Cu K_α radiation with a wavelength of 1.5406 Å. Scanning was done in the range of 2θ between 10° and 100°, with a step size of 0.02° and scan step time of 2 s and 19 s. The cell parameters were determined from the XRD patterns analysed by Rietveld refinement method using X'pert High score plus software.

3.3.2 Microstructural analysis

The microstructural analysis of films were done using field emission scanning electron microscopy (FE-SEM) (FEI Quanta 200F, Netherlands) operating at 20 kV. The energy dispersive X-ray spectrometer (EDAX) attached to the FESEM was used to determine the chemical composition of the samples. Before analyzing, all samples were coated with a Gold (Au) conductive layer in order to prevent charge build-up. The grain size and the film thickness of the sample were measured from the FESEM micrographs by using ImageJ software.

3.3.3 Electrical characterization

The voltage-current (V-I) characteristics of the thin film samples deposited on ITO coated glass substrate were measured. The multilayer coating was done in order to get the desired thickness. To pass the current through the film, it has to be made conducting on both the sides. A thin copper foil in the form of a rectangular shape placed in press contact mode on the oxide film surface was used as an electrode for the V-I characteristics measurements. The electrical connection was drawn from one of the corners of the copper foil and another from the ITO coated surface. A KEITHLEY 2400 source meter (21 V-1 A max. or 210 V-100 mA max.) was used to measure the V-I characteristics. The voltage was increased at constant intervals and the corresponding current readings were noted. The V-I characteristics thus obtained were plotted on graph.

5. RESULTS AND DISCUSSION

4.1 Thickness measurement

The thicknesses of the films were measured by using FESEM and Surface Profilometer (XP-Plus Stylus Profilometer, AMBIOS XP-200). The thickness of FESEM micrographs were measured by using ImageJ software and the FESEM cross-sectional micrographs for different number of layers of coating is shown in Fig. 4.2. The thickness of the films is in the range of 250-280 nm and 2.9-3.0 μm for three and thirty layers respectively. The variation of thickness of films with respect to number of layers is shown in Fig. 4.1. Surface Profilometer measures the thickness of films with reference to uncoated portion by contact method. The graphs for the thickness of films obtained by surface profilometer for different number of layers are shown in Fig. 4.3.
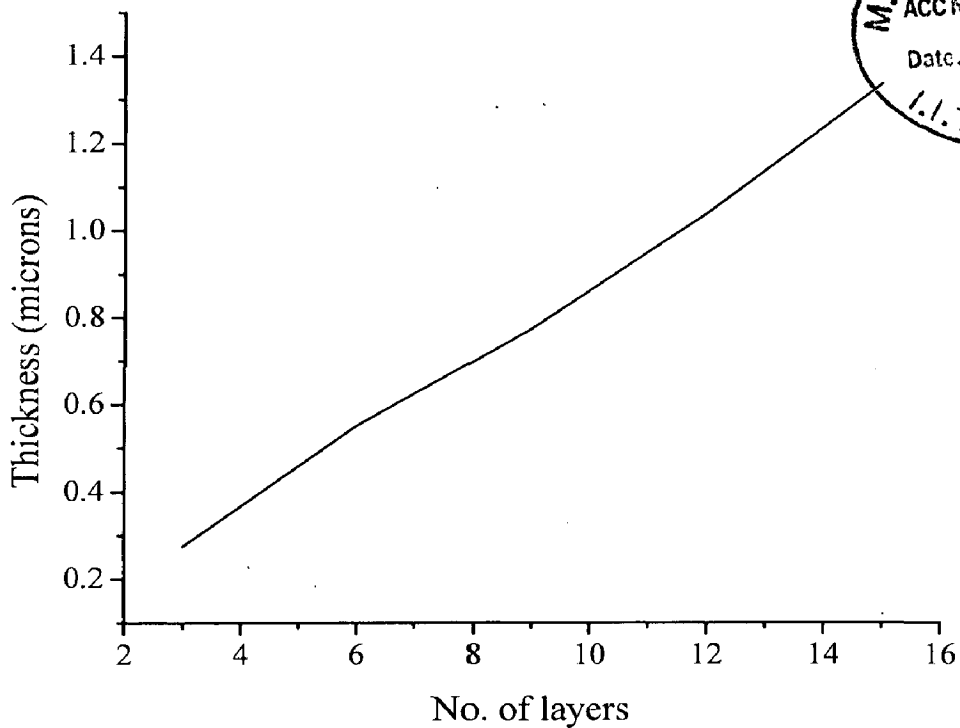
Fig. 4.1. Thickness of film with the number of layers of coating.
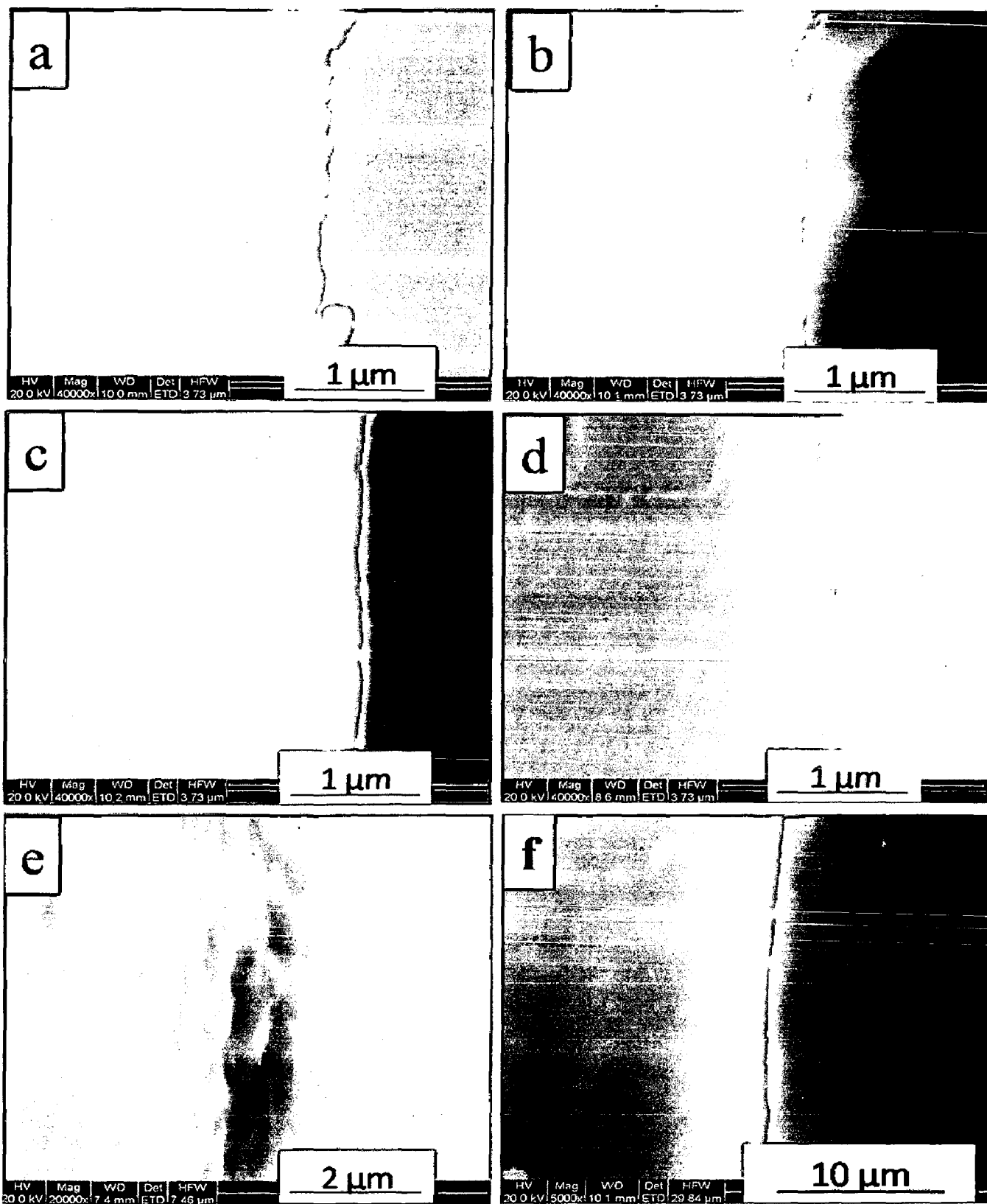
Fig. 4.2. FESEM micrographs of cross-section of ZnO based films of (a) 3 layers, (b) 6 layers, (c) 9 layers, (d) 12 layers, (e) 15 layers and (f) 30 layers.
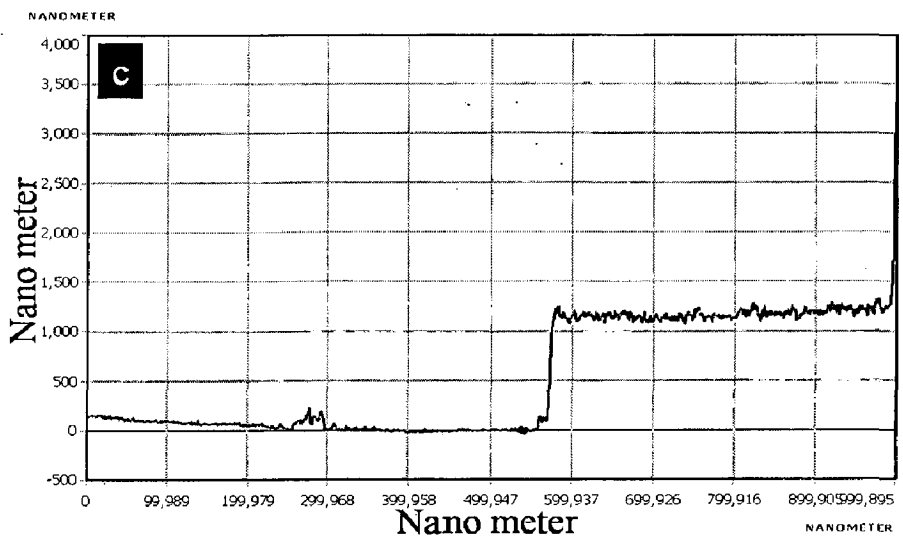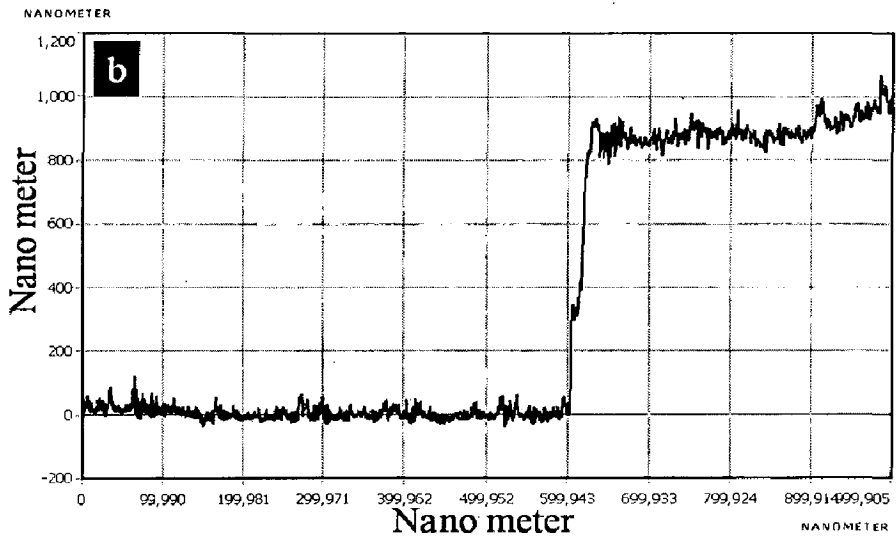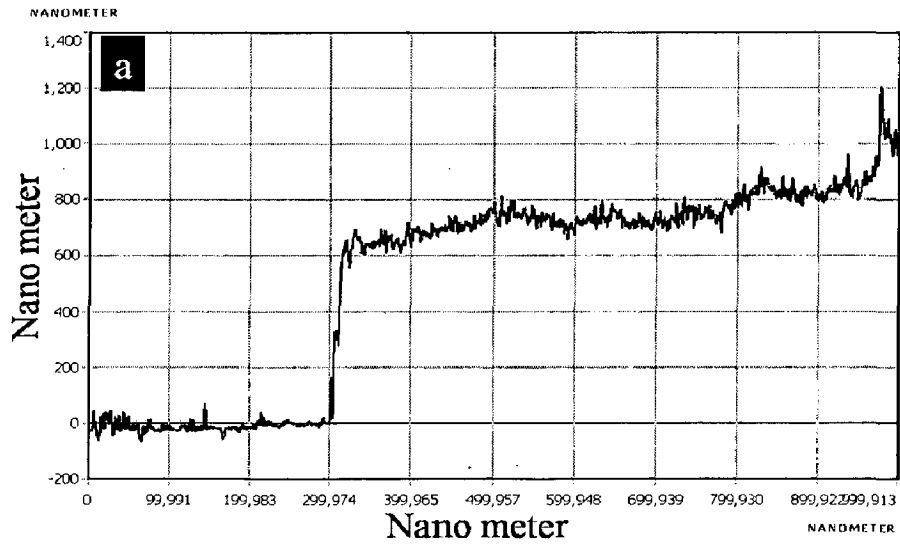
Fig. 4.3. Thickness plots of ZnO based films, (a) 9-layers coated film, (b) 12-layers coated film and (c) 15-layers coated film.

4.2 Crystal phases in ZnO-based ceramic films

Fig. 4.4 shows the X-ray diffraction (XRD) patterns of powder having (A) ZnO-0.5mol % V_2O_5 (ZV – pd) and (B) ZnO-0.5 mol% V_2O_5 and 0.5 mol% MnO (ZV 0.5M – pd). The diffraction peaks show ZnO as the major phase and $Zn_3(VO_4)_2$, the only secondary phase observed in (a) and no secondary phases were detected in (b).
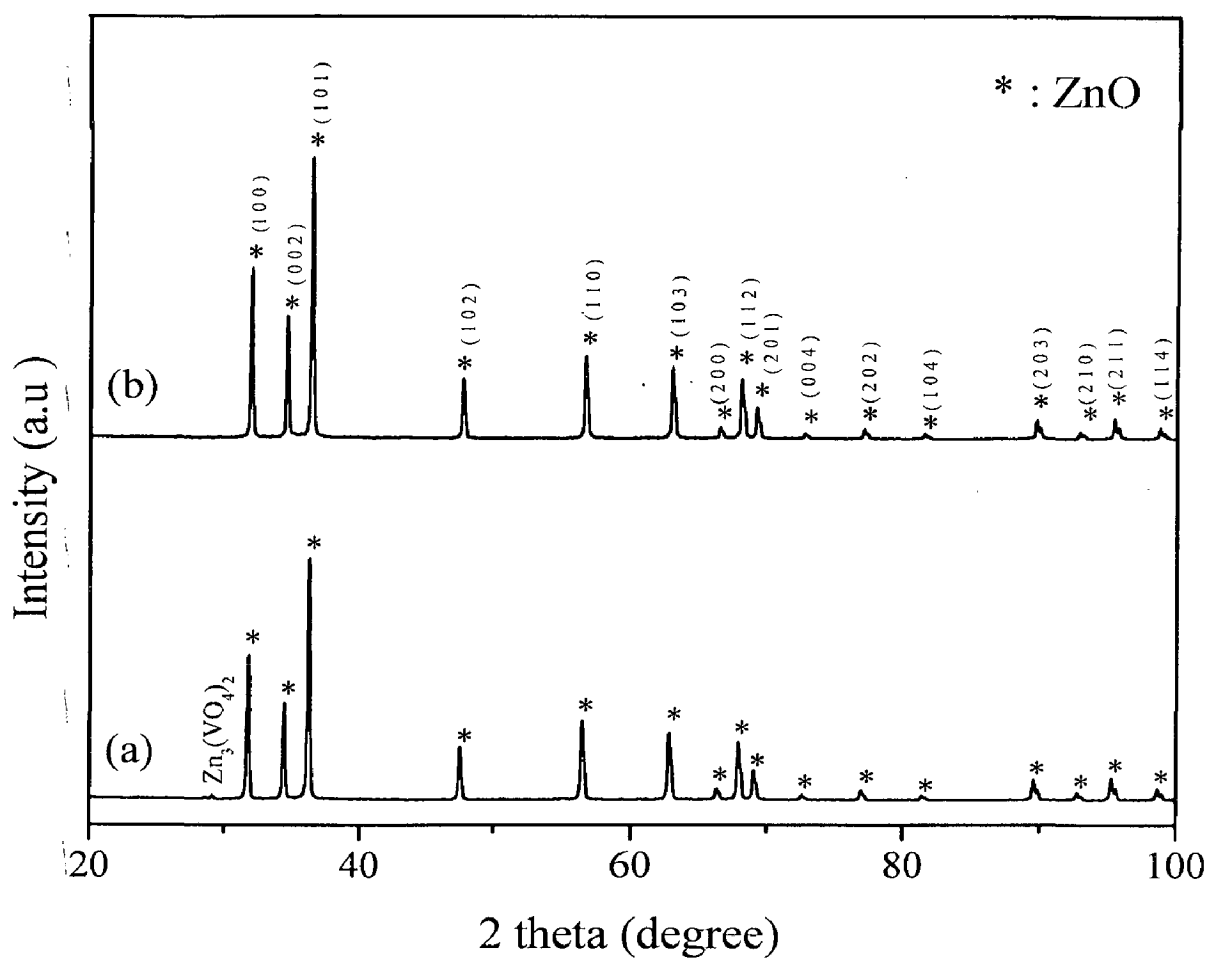
Fig. 4.4. XRD patterns of ZnO powder samples of (a) ZnO-0.5mol % V_2O_5 (ZV – pd) and (b) ZnO-0.5 mol% V_2O_5 and 0.5 mol% MnO (ZV 0.5M – pd).

Fig. 4.5 shows the XRD patterns of ZnO based thin films deposited by using sol with calcined powder dispersion (ZV-pdf) and sol without powder dispersion (ZV-2). No secondary phases related to V_2O_5 are detected in both the cases. So in order to save time and energy, sol without powder dispersion method of film preparation is adopted for further studies.
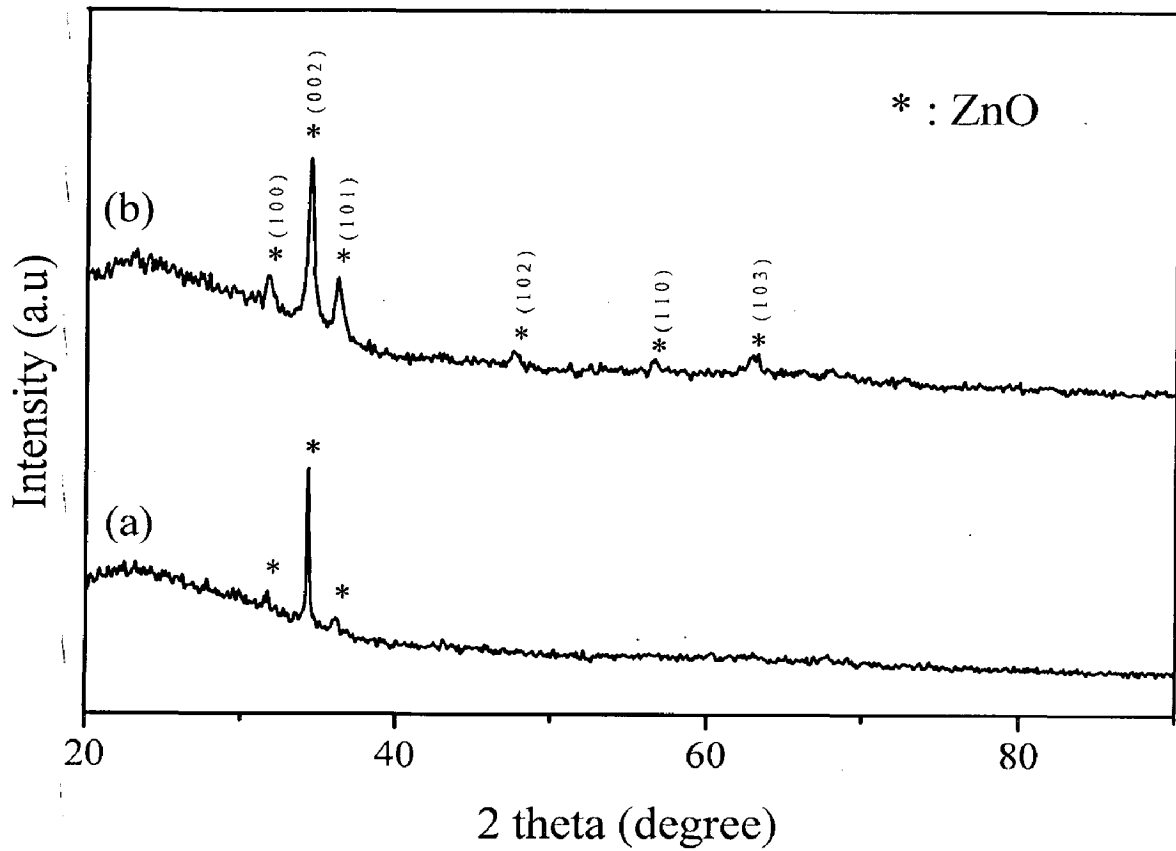

Fig. 4.5. XRD patterns of ZnO based thin films deposited by using different sols, (a) sol with calcined powder dispersion (ZV - pdf) and (b) sol without calcined powder dispersion (ZV - 2).

Fig. 4.6 shows XRD patterns of ZnO based thin films deposited with different layers. With the increase in number of layers, it is observed that the diffraction peaks of ZnO become sharp and intense, indicating the crystals of ZnO grown well. No secondary phases are detected for three layers coating. So the films were deposited for more than three layers.
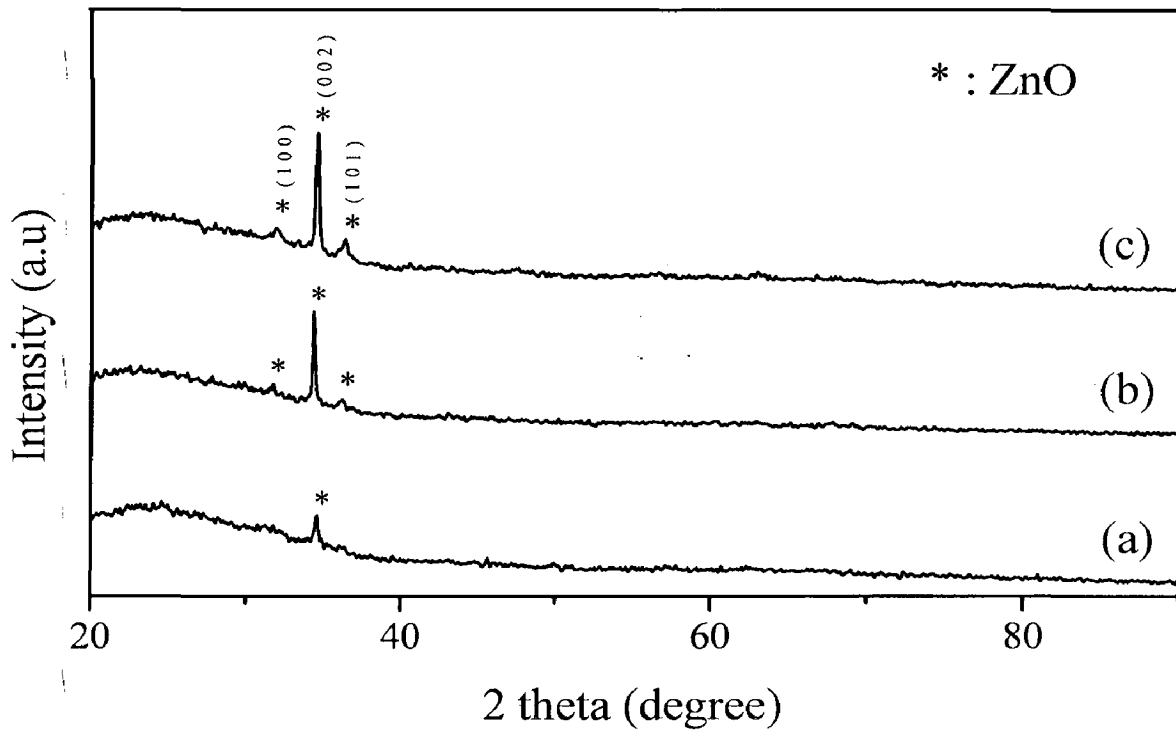

Fig. 4.6. XRD patterns of ZnO thin films of different layers, (a) one layer (ZV - 1), (b) two layers (ZV - 2) and (c) three layers (ZV - 3).

Fig. 4.7 shows the XRD patterns of ZnO based thin films annealed at 550°C for different time periods. All the peaks in the pattern are of ZnO. It has been observed that as the annealing time increases, the ZnO peaks become sharper but no secondary phases detected. The XRD patterns shown are of samples of 17 layers but not subjected to any heating after each layer. From this study it is concluded that calcination is required after each layer in order to get intense and sharp peaks of ZnO and secondary phases.
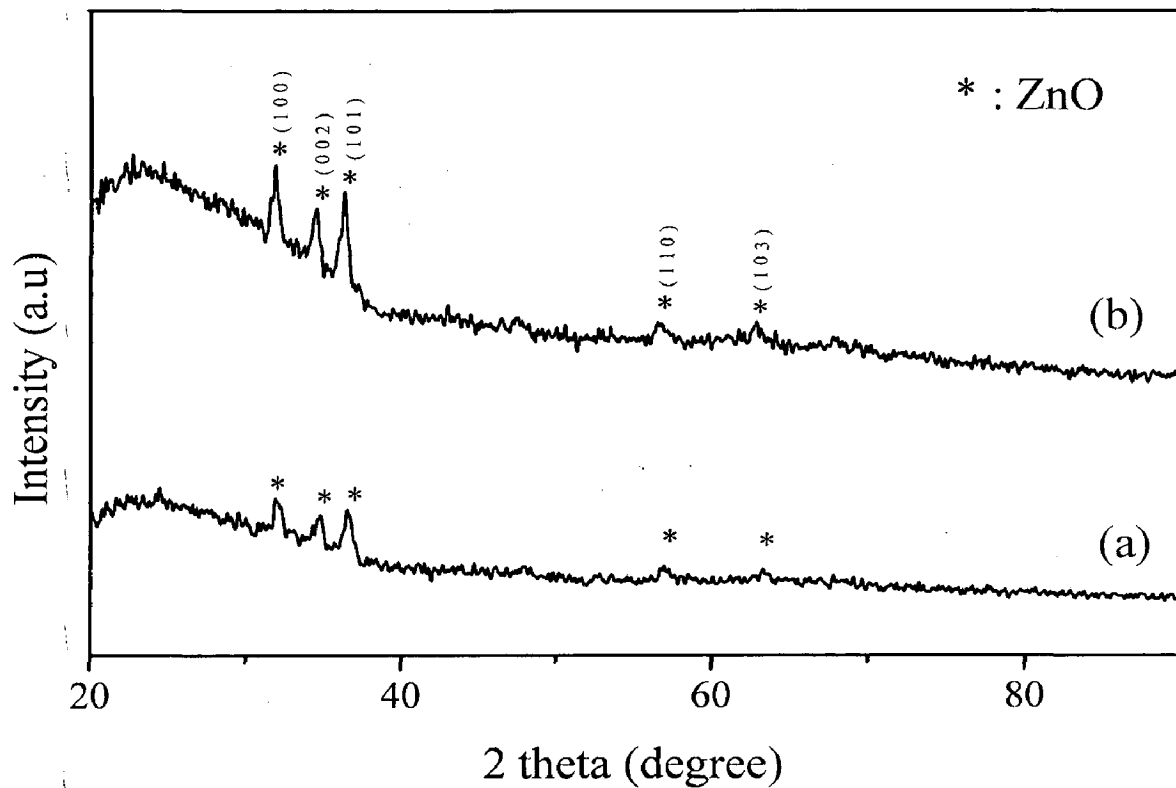

Fig. 4.7. XRD patterns of ZnO based thin films annealed for different time periods, (a) 30 min. (ZV1.0M - 3) and (b) 90 min. (ZV 1.0M - 4).

Fig. 4.8 shows the XRD patterns of ZnO based thin films annealed at different temperatures. The XRD patterns are of the same sample examined after annealing at 350°C and 550°C for 30 min. It is observed that the relative intensity of peaks increases with the increase in the annealing temperature and an additional phase of MnO was found in the sample annealed at 550°C.
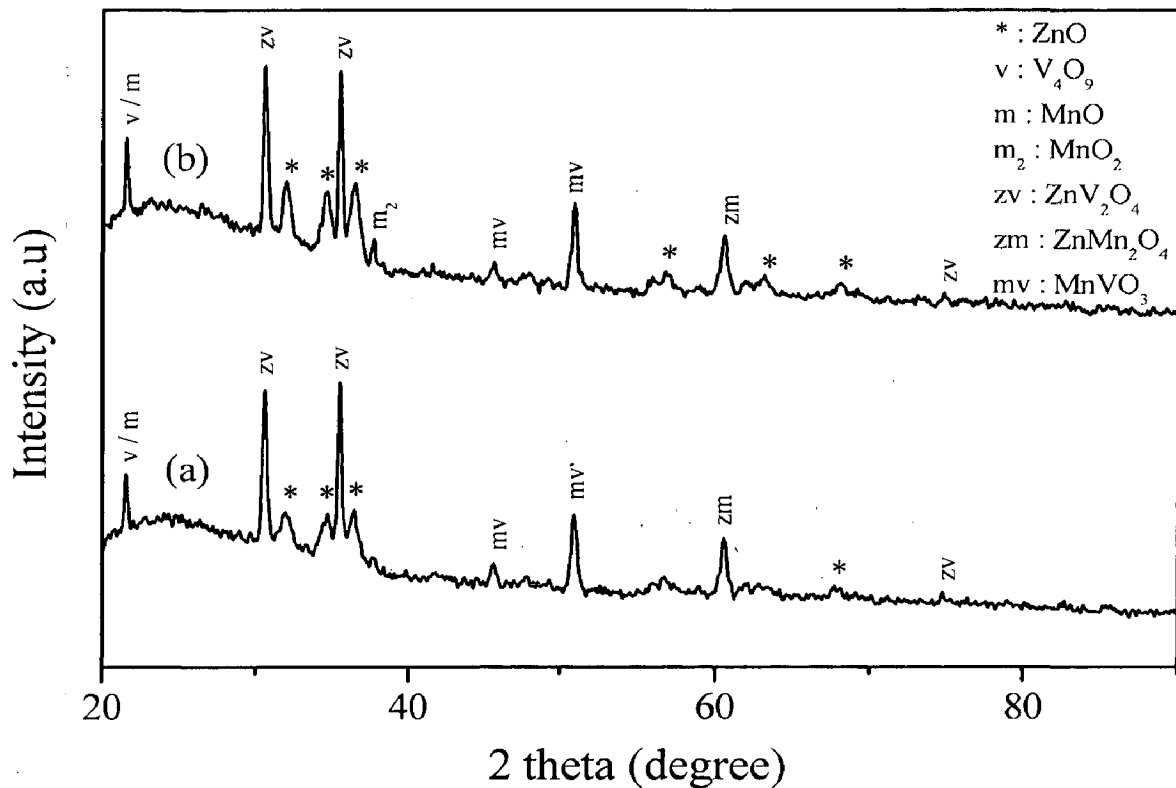

Fig. 4.8. XRD patterns of ZnO based thin films for different annealing temperature, (a) annealed at 350°C (ZV 1.0M - 1) and (b) annealed at 550°C (ZV 1.0M - 2).

Fig. 4.9 shows the XRD patterns of ZnO based thin films doped with different mol% of MnO. The XRD patterns show no changes in intensity or in secondary phase detection. Similar observations were reported for different MnO contents [6].
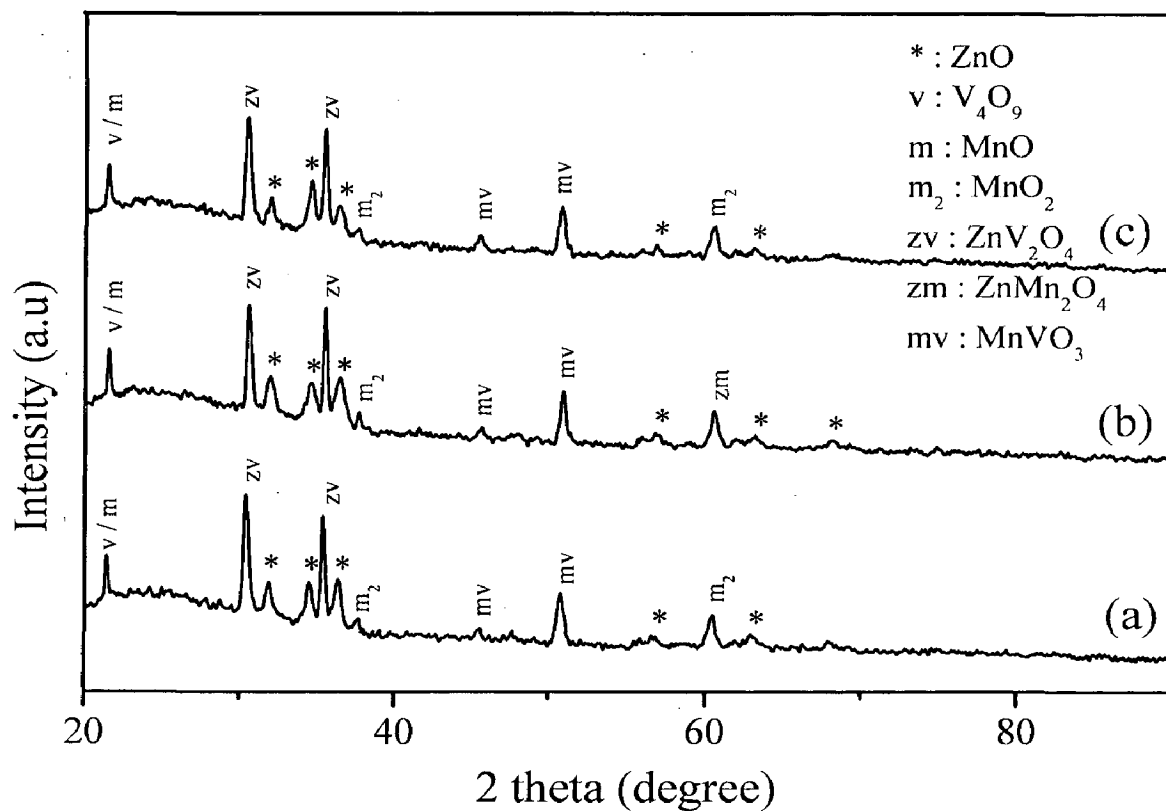

Fig. 4.9. XRD patterns of ZnO based thin films having ZnO-0.5 mol% V_2O_5 and (a) 0.5 mol% MnO (ZV 0.5M - 1), (b) 1.0 mol% MnO (ZV 1.0M - 2) and (c) 1.5 mol% MnO (ZV 1.5M - 1).

Fig. 4.10 shows the XRD patterns of ZnO based thin films annealed at different temperatures. The secondary phases $Zn_3(VO_4)_2$ and $Zn_4V_2O_9$ were observed from the sample which were annealed at 700°C. The phases $Zn_3(VO_4)_2$ and $Zn_4V_2O_9$, identified from the patterns of ICSD data file (00-011-0288) and (01-077-1757) respectively. The appearance of the $Zn_3(VO_4)_2$ and $Zn_4V_2O_9$ phases were consistent with earlier reports of V_2O_5-MnO-doped ZnO ceramics sintered at 900°C [12-14,17]. It was suggested that the existence of these minority secondary phases have an effect on the electrical properties.
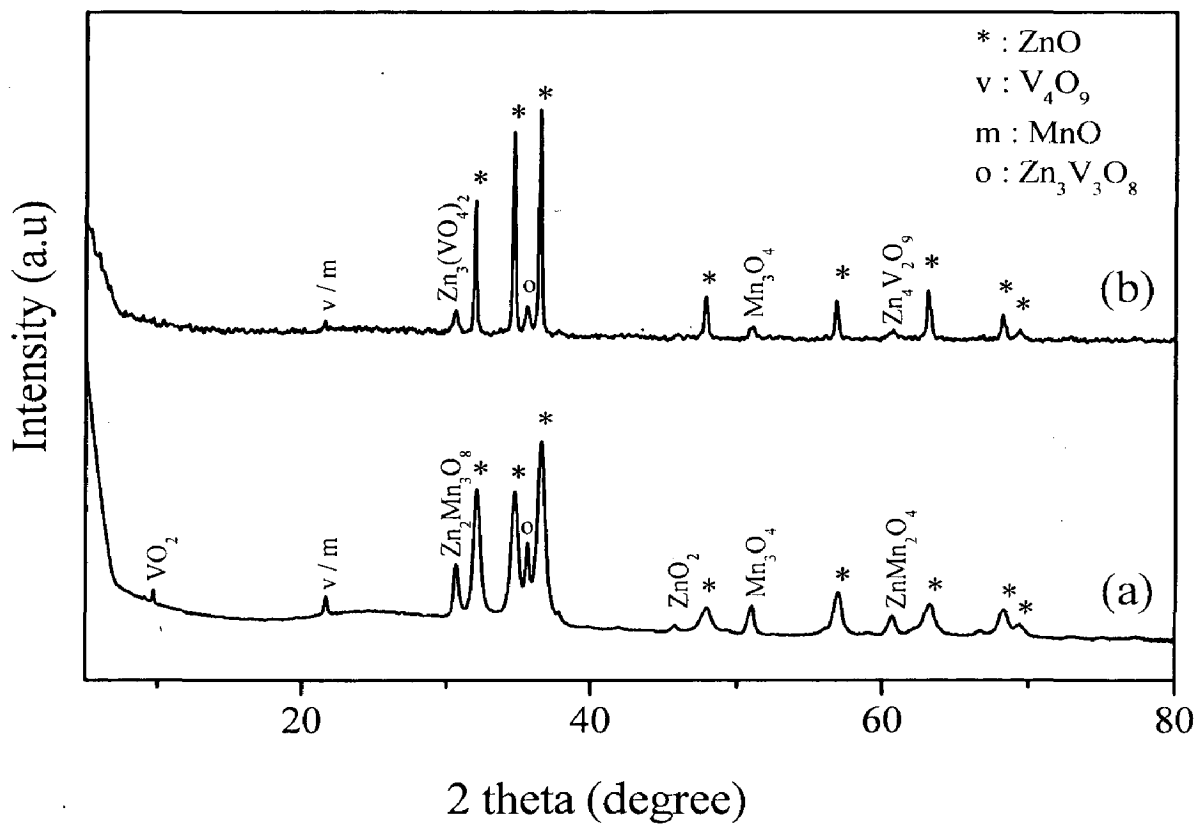

Fig. 4.10. XRD patterns of ZnO based thin films of ZnO-0.5 mol% V_2O_5 and 1.5 mol% MnO (a) annealed at 550°C (ZV 1.5M - 5) and (b) annealed at 700°C (ZV 1.5M - 6).

Fig. 4.11 shows the XRD patterns of pure ZnO thin films annealed at different temperatures. The peaks in the pattern are of ZnO and $In_{1.94}Sn_{0.06}O_3$. The $In_{1.94}Sn_{0.06}O_3$ peaks observed may be because of ITO coated glass substrate.
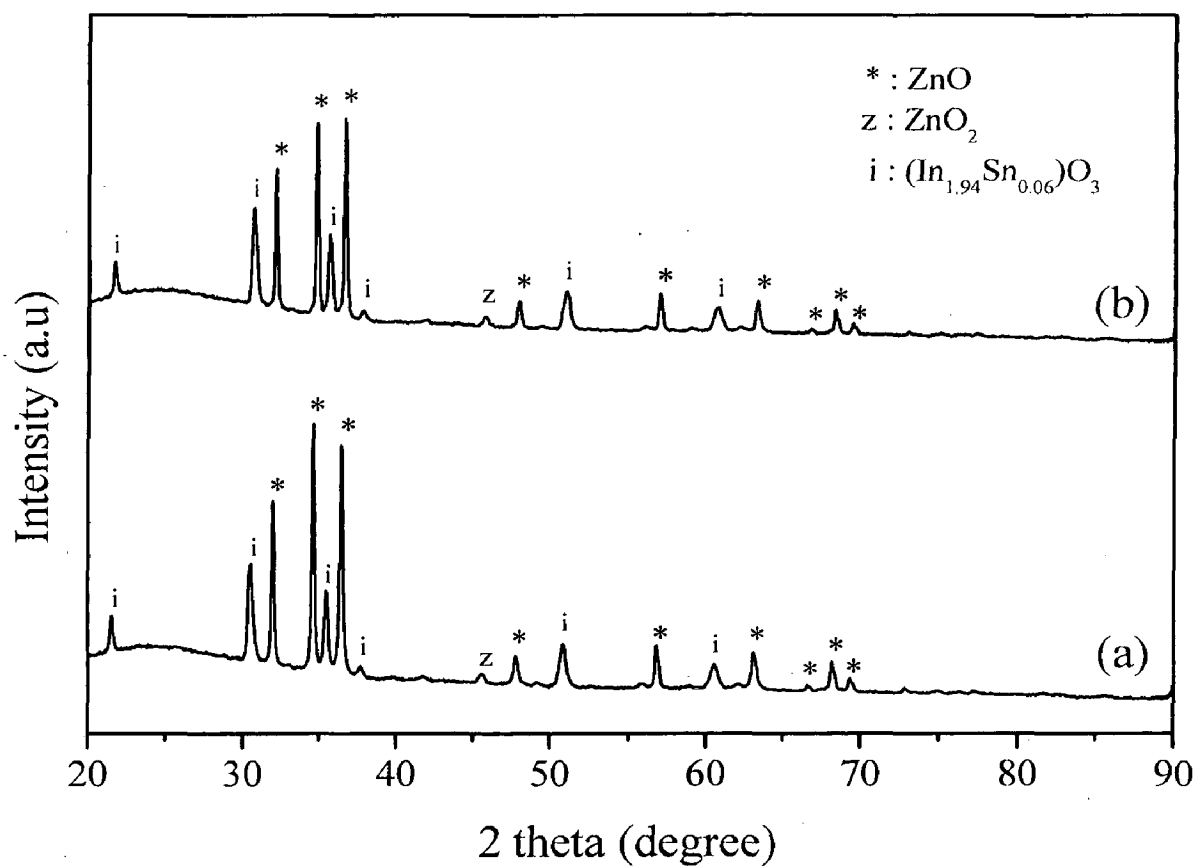

Fig. 4.11. XRD patterns of pure ZnO thin films, (a) annealed at 550°C (Z - 1) and (b) annealed at 700°C (Z - 2).

Fig. 4.12 shows the XRD patterns of undoped and doped ZnO (ZnO-0.5 mol% V_2O_5 and 1.5 mol% MnO) based thin films. The doped ZnO film pattern show peaks of ZnO and secondary phases related to V_2O_5 and MnO, indicating that the synthesis conditions, used in this study, are favorable.
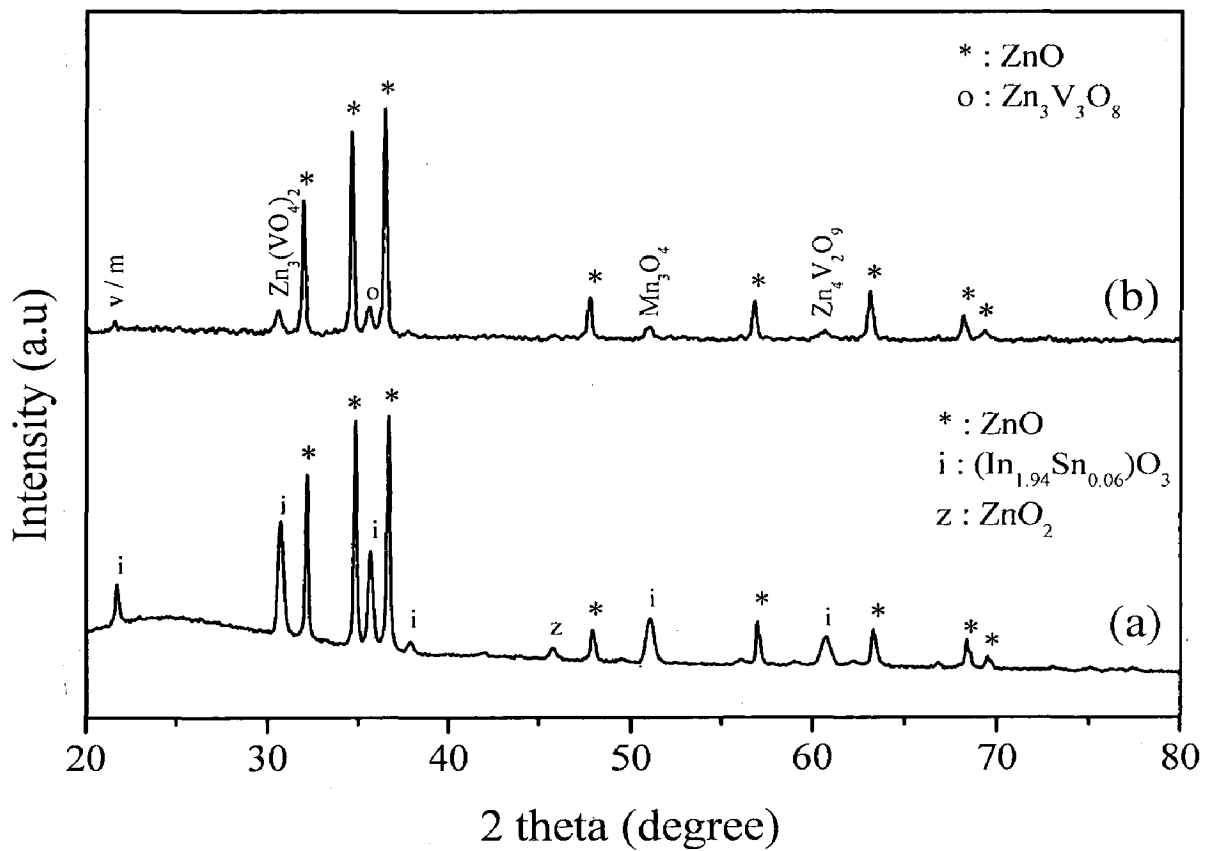

Fig. 4.12. XRD patterns of ZnO based thin films, (a) undoped (Z - 2) and (b) doped (ZV 1.5M - 6).

4.3 Microstructural characterization

Fig. 4.13 shows FESEM micrographs of the surface of 100% ZnO based films annealed at 550°C and 700°C respectively. The grain size of the sample is determined by using ImageJ software. The grain sizes are in the range of 50-70 nm and 90-110 nm for the samples annealed at 550°C and 700°C respectively. The micrographs show fibre like structure at higher magnification. The EDAX analysis for the same samples is shown in Fig. 4.14. Peaks related to Indium and Tin was also detected along with Zinc peaks because of ITO coated glass substrate.
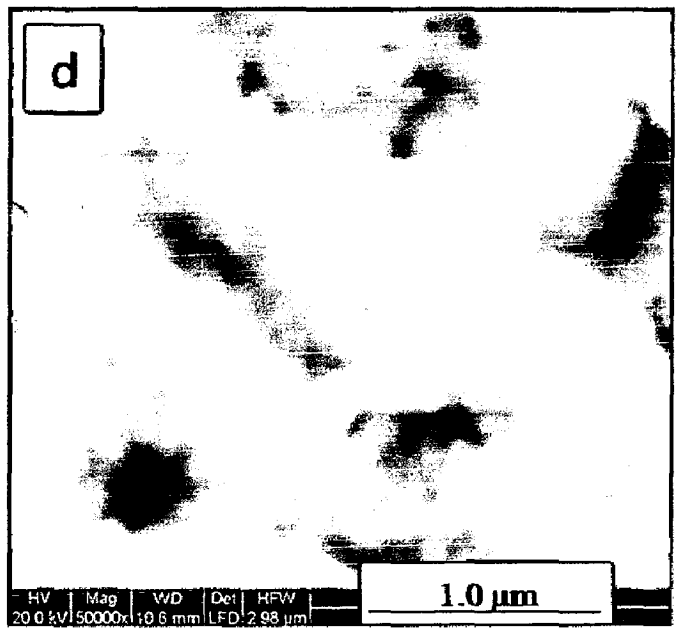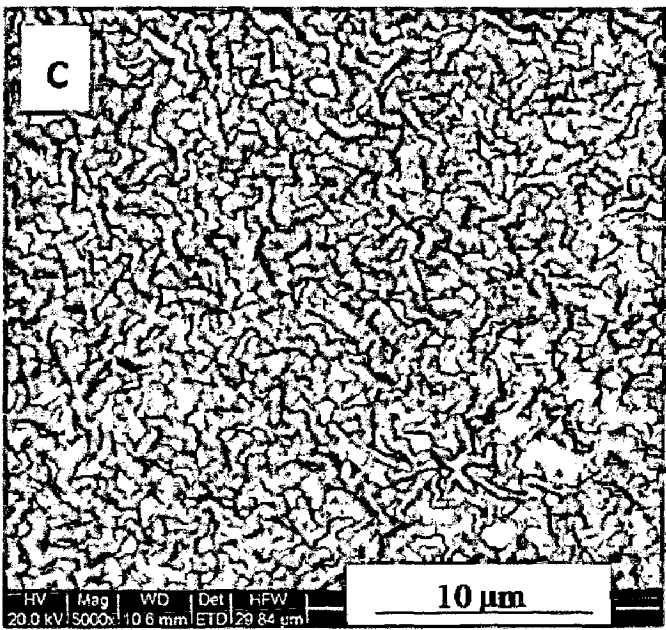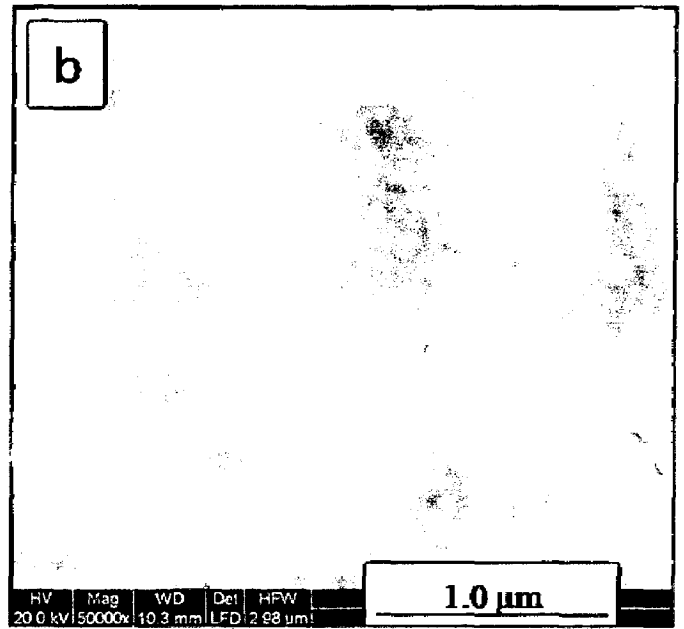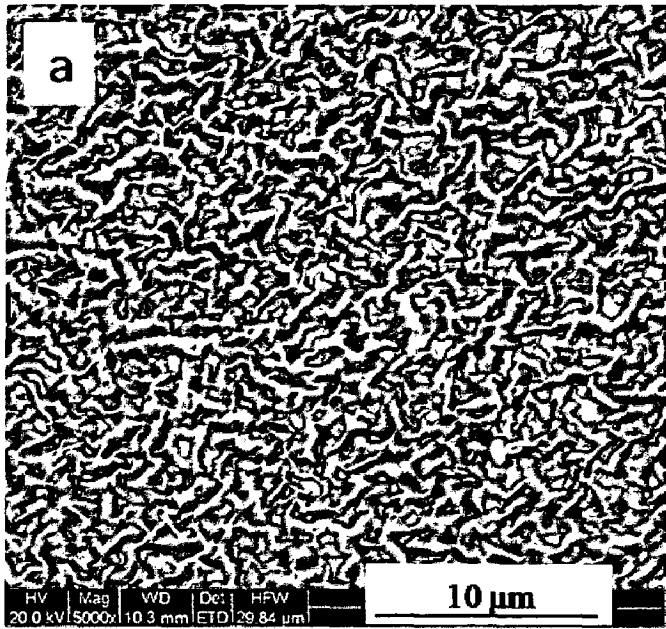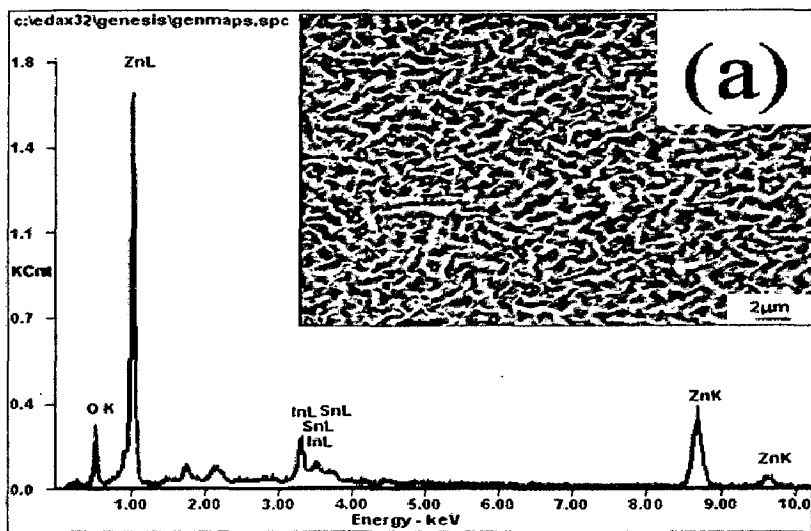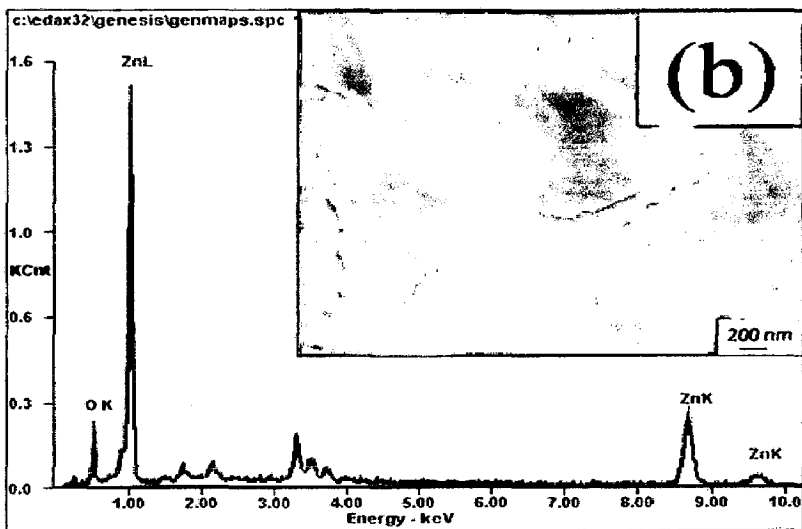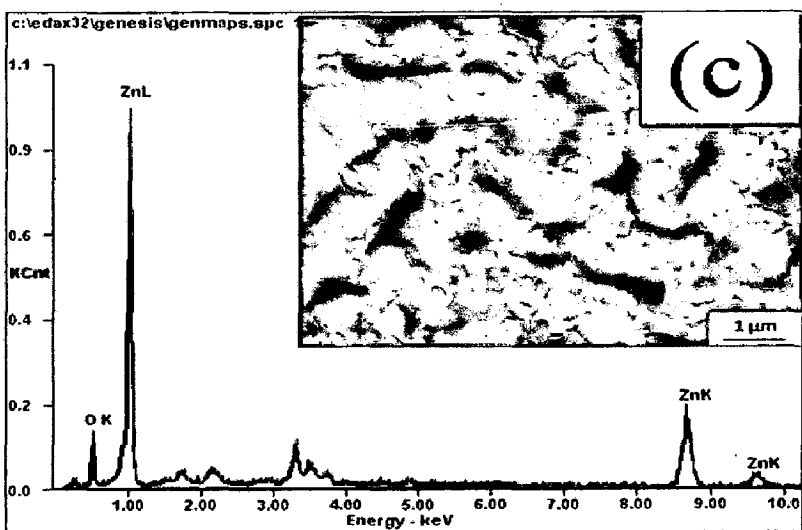
Fig. 4.13. FESEM micrographs of the surface of pure ZnO films, (a, b) annealed at 550°C (Z-1) and (c, d) annealed at 700°C (Z-2).

Element	Wt%	At%
OK	15.62	45.51
InL	17.39	07.06
SnL	01.05	00.41
ZnK	65.94	47.02
Matrix	Correction	ZAF

Element	Wt%	At%
OK	15.29	42.45
ZnK	84.71	57.55
Matrix	Correction	ZAF

Element	Wt%	At%
OK	13.21	38.33
ZnK	86.79	61.67
Matrix	Correction	ZAF

Fig. 4.14. EDAX microanalysis of the surface of pure ZnO films, (a, b) annealed at 550°C (Z-1) and (c) annealed at 700°C (Z-2).

Fig. 4.15 shows FESEM micrographs of the surface of ZnO based thin films of ZnO-0.5 mol% V_2O_5 and 1.5 mol% MnO, annealed at 550°C for different time periods such as 60 min, 120min and 180 min. The morphology of these samples has elongated fibre like textures at the magnifications observations were made. So fibre diameter is used as the index for the grain size measurement. At some still higher magnifications grains were seen in the case of Fig. 4.13. From the micrographs it is observed that there is not much effect of annealing time. The average fibre diameter is in the range of 700-900 nm for all the three samples. The EDAX analysis for the same samples is shown in Figure 4.16. EDAX data shows that the elemental composition of the analysed area which implies that Zn as the major constituent, followed by O, Mn and V in the decreasing order. From reference [14], it is known that the Mn is present uniformly throughout the sample and V at triple junctions and grain boundaries. This is evident from the EDAX data, where percent of Mn is greater than percent of V which can be inferred as Mn is present inside grain whereas V is present at grain boundary.
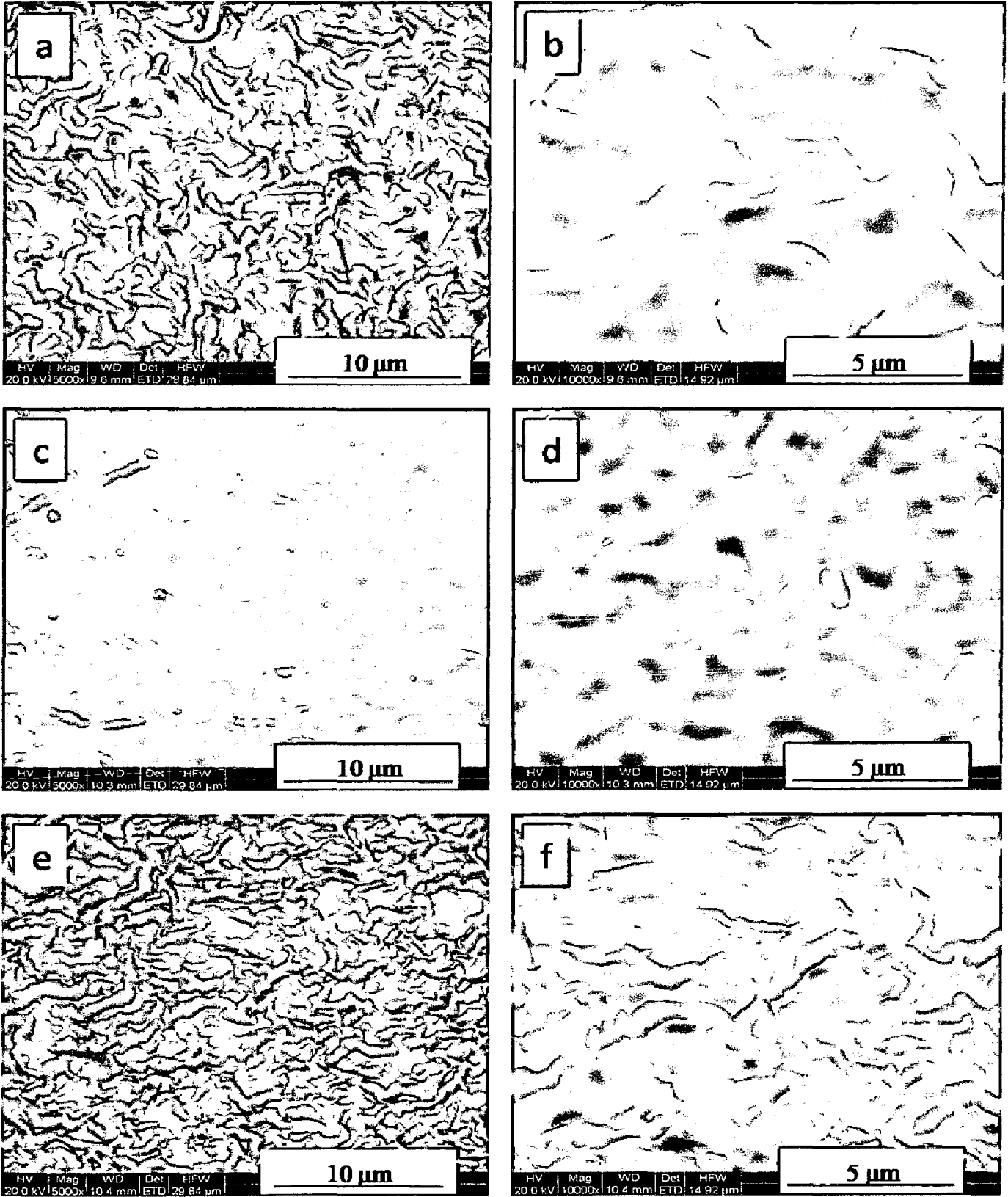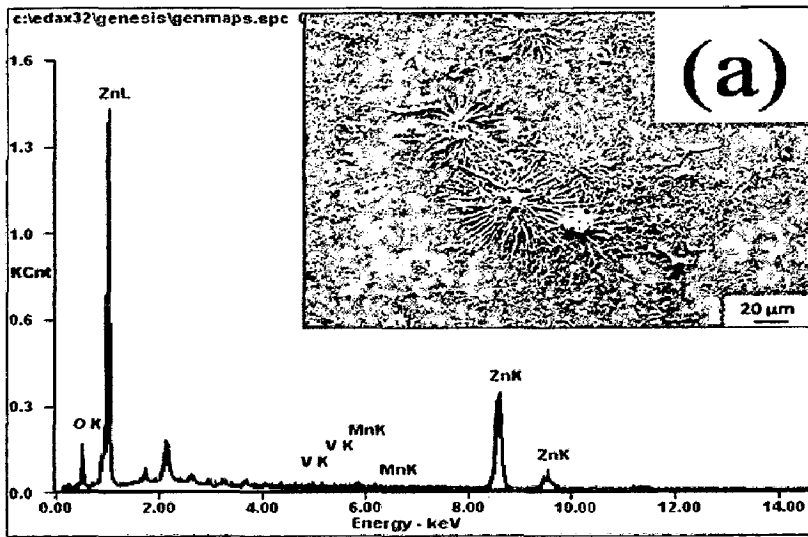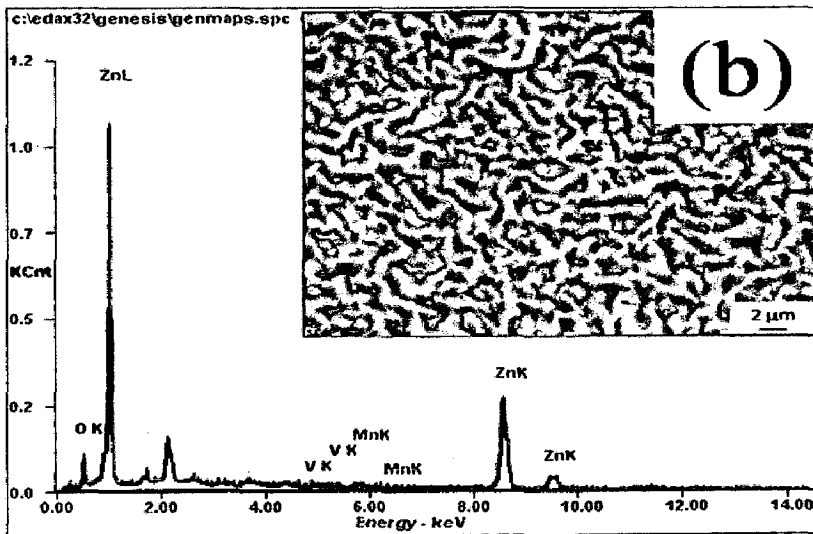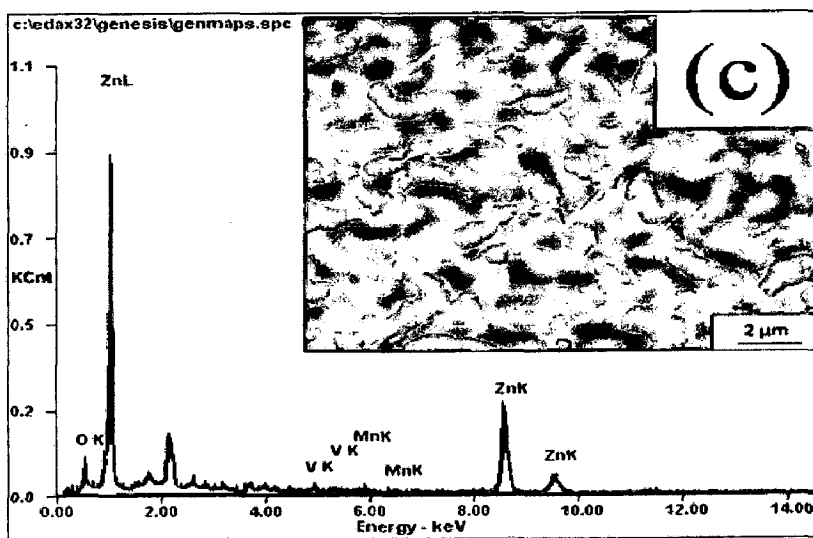
Fig. 4.15. FESEM micrographs of the surface of ZnO based films annealed at 550°C for (a, b) 60 min (ZV 1.5M - 2), (c, d) 120 min (ZV 1.5M - 3) and (e, f) 180 min (ZV 1.5M - 4).

Table (a):

Element	Wt%	At%
OK	09.07	28.83
VK	00.90	00.90
MnK	01.40	01.30
ZnK	88.63	68.96
Matrix	Correction	ZAF

Table (b):

Element	Wt%	At%
OK	08.42	27.24
VK	00.72	00.73
MnK	00.65	00.61
ZnK	90.20	71.41
Matrix	Correction	ZAF

Table (c):

Element	Wt%	At%
OK	08.66	27.76
VK	01.49	01.50
MnK	01.58	01.47
ZnK	88.27	69.27
Matrix	Correction	ZAF

Fig. 4.16. EDAX microanalysis of the surface of ZnO based films annealed at 550°C for, (a, b) 60 min (ZV 1.5M - 2) and (c) 120 min (ZV 1.5M - 3).

Fig. 4.17 shows FESEM micrographs of the surface of ZnO based thin films of ZnO-0.5 mol% V_2O_5-1.5 mol% MnO, annealed at 550°C and 700°C. The grain size of films annealed at 550°C and 700°C are in the range of 25-40 nm and 70-90 nm respectively, indicating that grain size increases with the increase in annealing temperature. The average grain size of doped ZnO films are smaller than the grain size of 100% ZnO films annealed at the respective temperature indicating that the addition of dopants inhibited the grain growth. The morphology and distribution of the additives could not be observed clearly because their grains were very small. The EDAX analysis for the same samples is shown in Fig. 4.18.
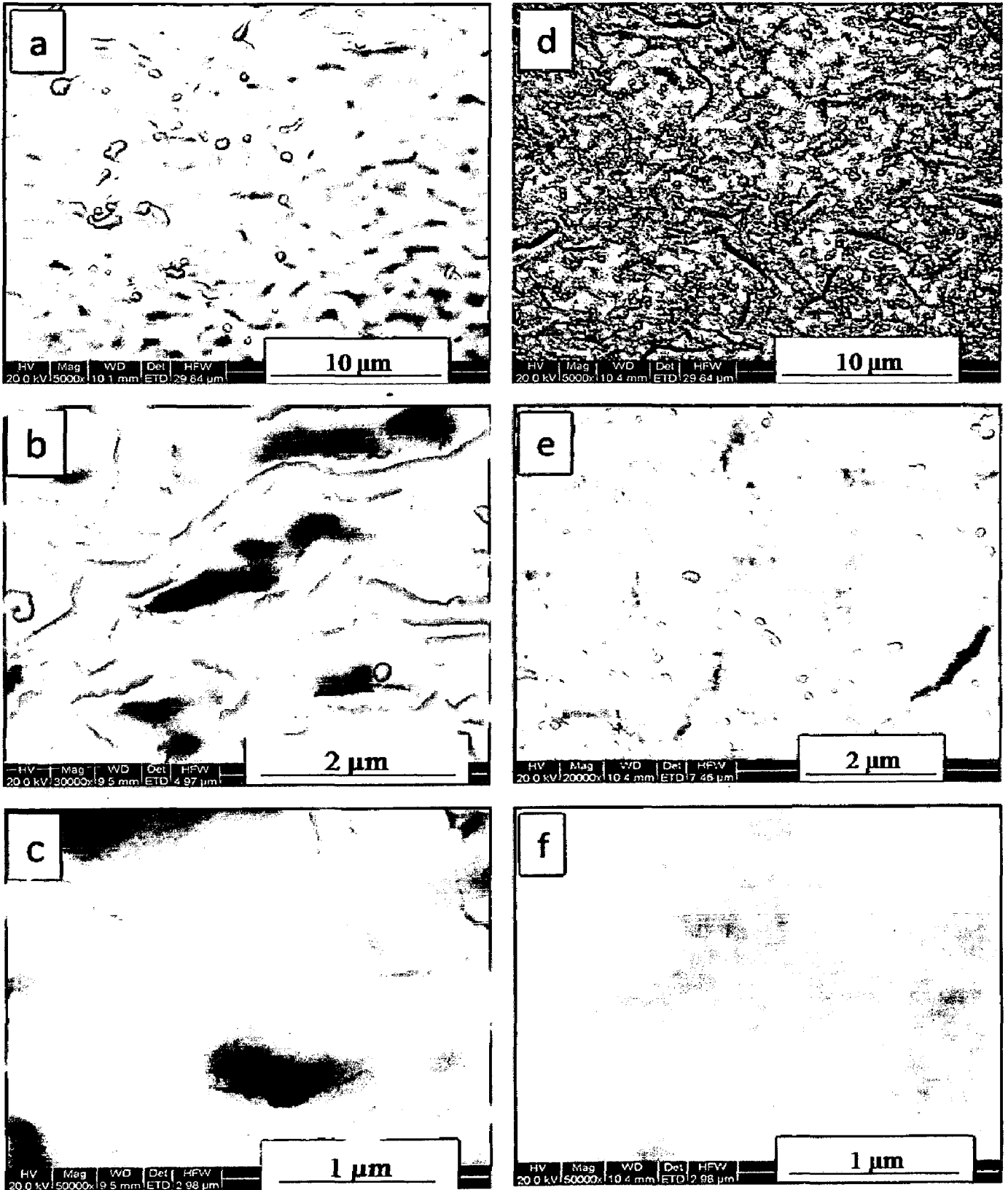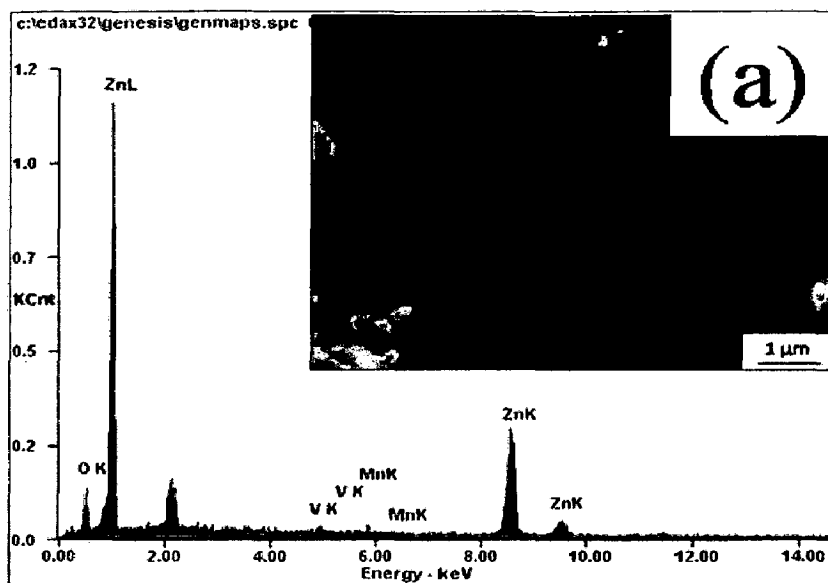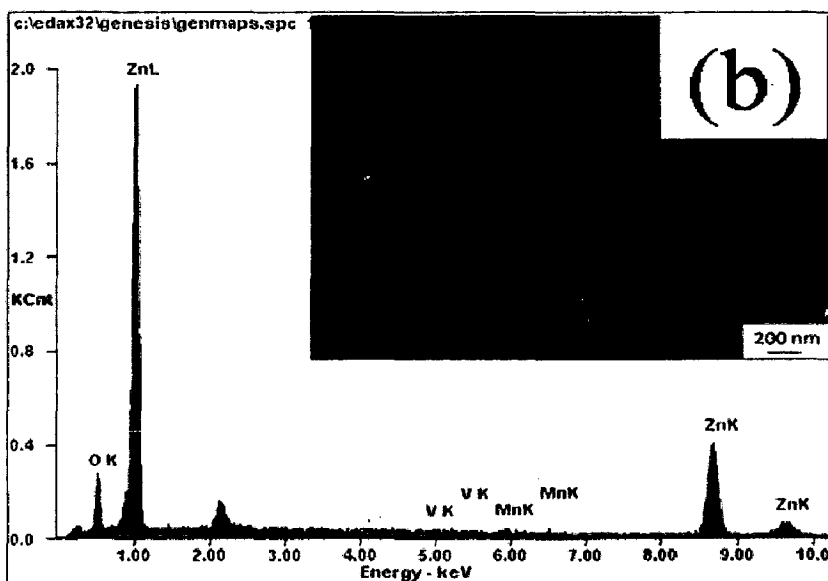
Fig. 4.17. FESEM micrographs of the surface of ZnO based films annealed at (a, b, c) 550°C (ZV 1.5M - 5) and (d, e, f): 700°C (ZV 1.5M - 6).

Element	Wt%	At%
OK	08.70	27.87
VK	01.37	01.38
MnK	01.43	01.34
ZnK	88.50	69.42
Matrix	Correction	ZAF

Element	Wt%	At%
OK	12.49	36.73
VK	00.72	00.67
MnK	01.19	01.02
ZnK	85.60	61.59
Matrix	Correction	ZAF

Fig. 4.18. EDAX microanalysis of the surface ZnO based films annealed at (a) 550°C (ZV 1.5M - 5) and (b) 700°C (ZV 1.5M - 6).
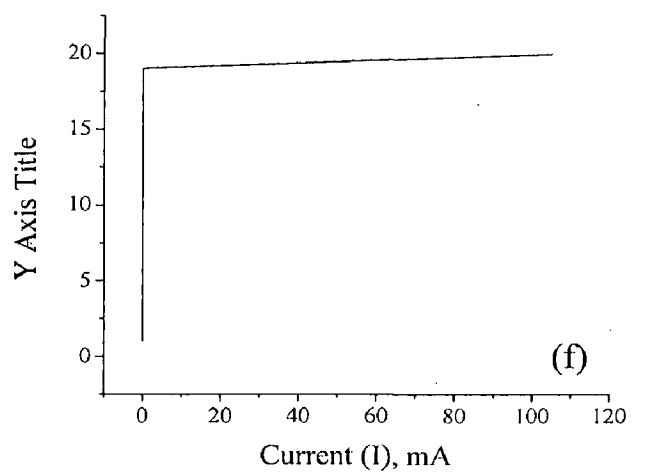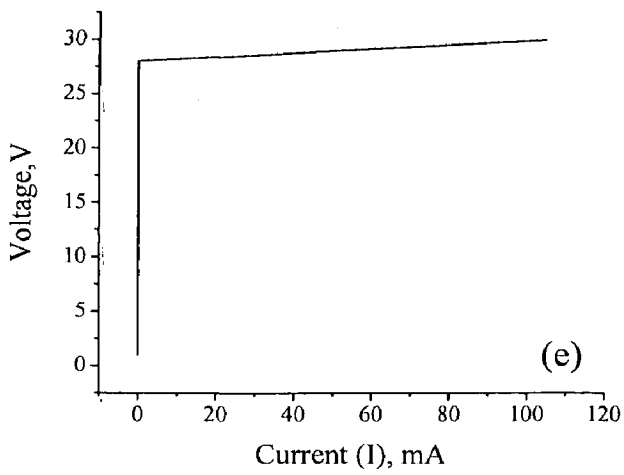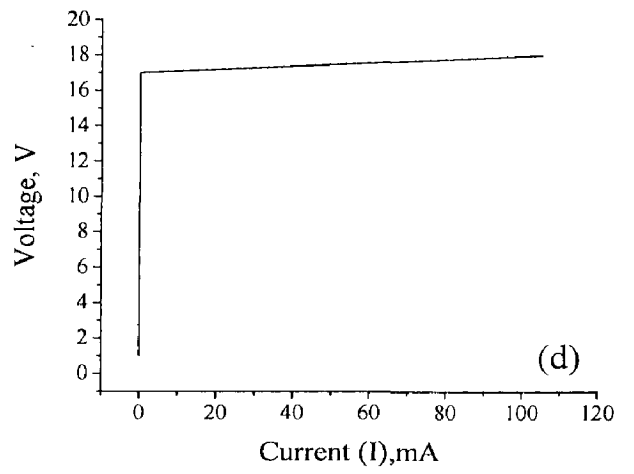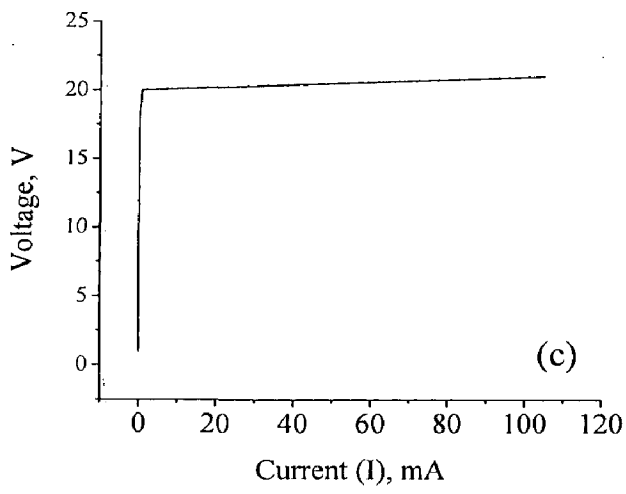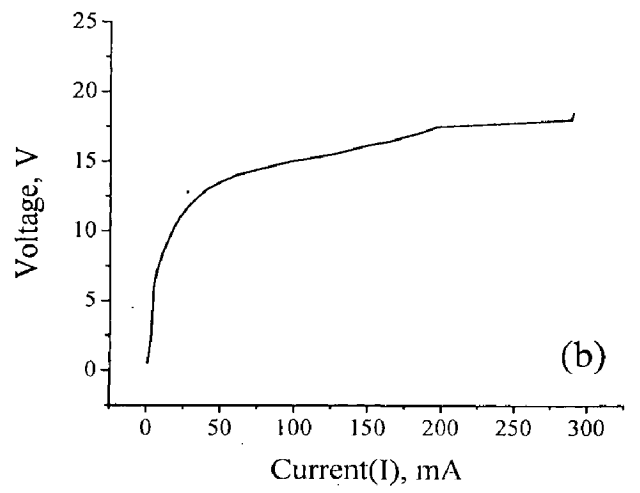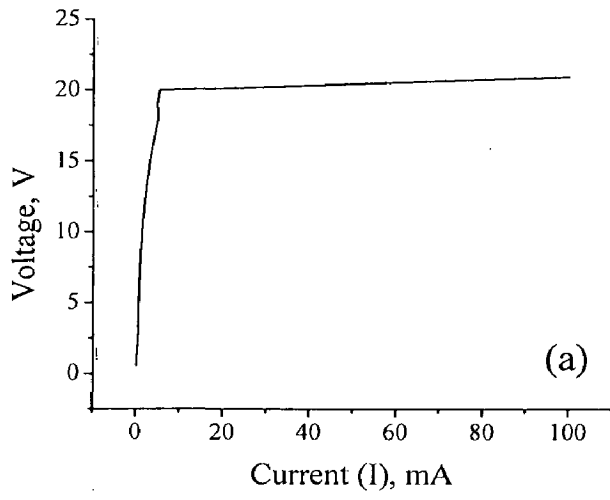
4.4 Electrical characterization

Fig. 4.19 shows the V-I characteristics of ZnO based ceramic films. The V-I characteristics of the ZnO based ceramic films developed with different number of layers and annealed at two different temperatures is summerzed in Table 4.1. A KEITHLEY 2400 source meter was used to measure the V-I characteristics and V-I plots were drawn from the source meter readings. The non linear behaviour of the V-I is evident from these plots and the non linear coefficient, α, is calculated from the non ohmic region of the plots.

There is a limitation to which the Keithley 2400 source meter can measure current. For values of voltage ranging from 0-21 volts, the current can be measured up to 1 A, whereas, for voltage values ranging from 0-210 volts, the maximum value of current that can be measured is 100 mA. Due to this limitation, maximum current reading noted is 104.99 mA and the same value is considered as I_2 value for the calculation of α.

Doped ZnO films show higher non linear coefficient (α) compared to the undoped ZnO samples. The samples annealed at 700°C shows higher α values and lower breakdown voltage compared to the samples annealed at 550°C. The higher α values for samples annealed at 700°C are attributed to the presence of secondary phases $Zn_3(VO_4)_2$ and $Zn_4V_2O_9$ and lower breakdown voltage is due to the larger grain size resulted in due to higher annealing temperature.

Table 4.1. Nonlinear coefficient (α) of the ZnO based thin films prepared by varying the number of layer and annealing temperature

Sample no.	Composition (mol %) ZnO:V_2O_5:MnO	No. of layers	Pyrolysed at (°C)	Soaking time (min)	Annealed at (°C)	Soaking time (min)	Breakdown Voltage, V_B	Nonlinear coefficient, α
1	100 : 0.0 : 0.0	12	240	10	550	60	19	55
2	100 : 0.0 : 0.0	12	240	10	700	60	17.5	14
3	99.0 : 0.5 : 1.5	10	240	10	550	60	20	103
4	99.0 : 0.5 : 1.5	10	240	10	700	60	17	156
5	99.0 : 0.5 : 1.5	15	240	10	550	60	28	134
6	99.0 : 0.5 : 1.5	15	240	10	700	60	19	177
7	99.0 : 0.5 : 1.5	20	240	10	550	60	35	222
8	99.0 : 0.5 : 1.5	20	240	10	700	60	24	248
9	99.0 : 0.5 : 1.5	25	240	10	550	60	44	279
10	99.0 : 0.5 : 1.5	25	240	10	700	60	31	313
11	99.0 : 0.5 : 1.5	30	240	10	550	60	57	347
12	99.0 : 0.5 : 1.5	30	240	10	700	60	42	420
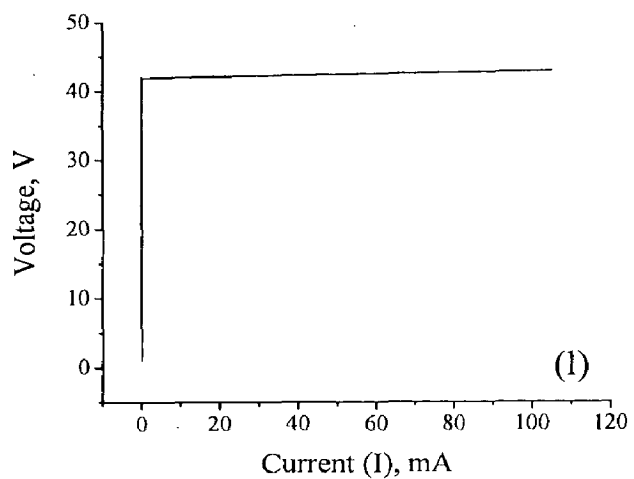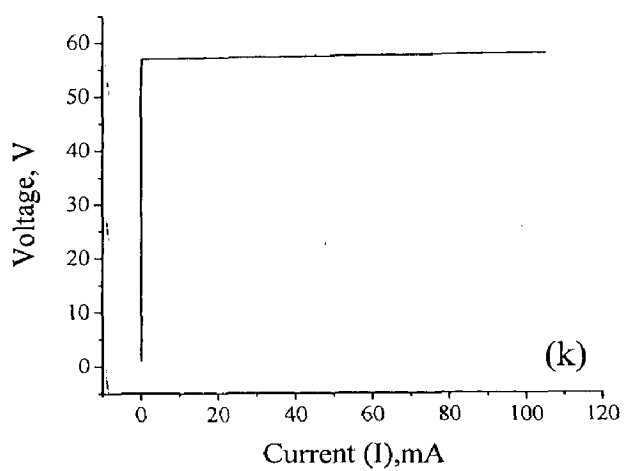
Fig. 4.19. V-I characteristics of ZnO based films of samples, (a) 1, (b) 2, (c) 3, (d) 4, (e) 5, (f) 6, (g) 7, (h) 8, (i) 9, (j) 10, (k) 11 and (l) 12.

6. CONCLUSIONS

Ceramic oxide films in the system ZnO-0.5 mol% V_2O_5-x mol% MnO (x = 0.5, 1.0, 1.5) were prepared by sol-gel process for low voltage varistors preparation. The following conclusions can be drawn from the present study:

1. ZnO based films having thickness varying from 0.25 μm to 3 μm have been developed successfully by sol-gel method.

2. XRD patterns show the formation of ZnO phase along with a few minority secondary phases.

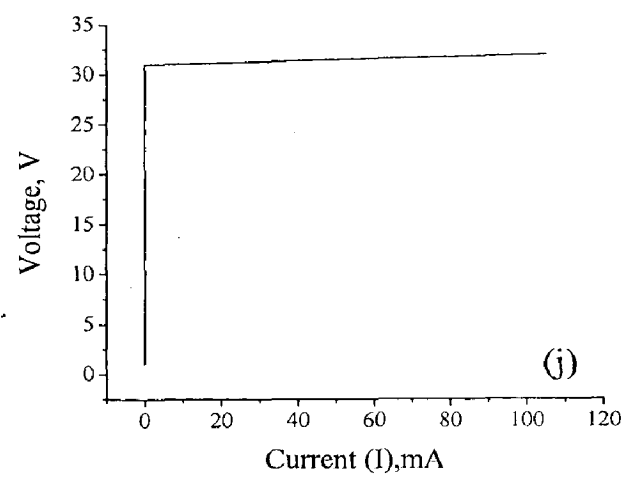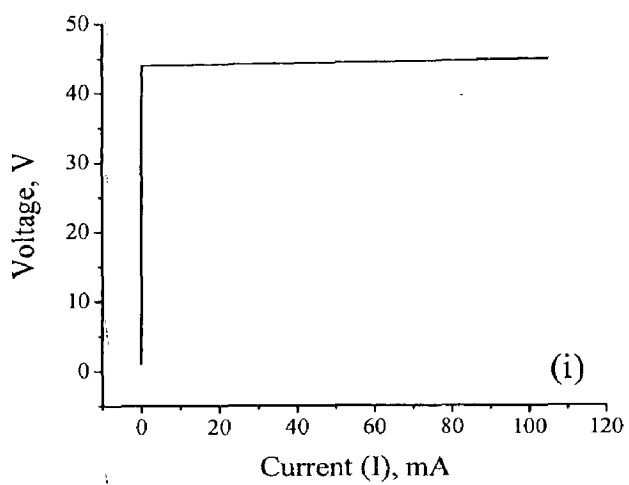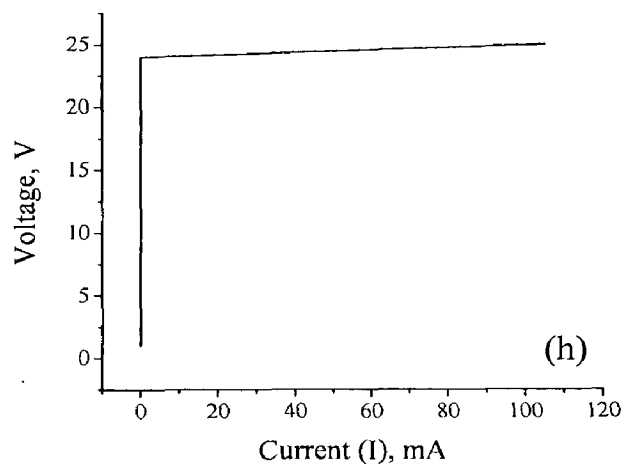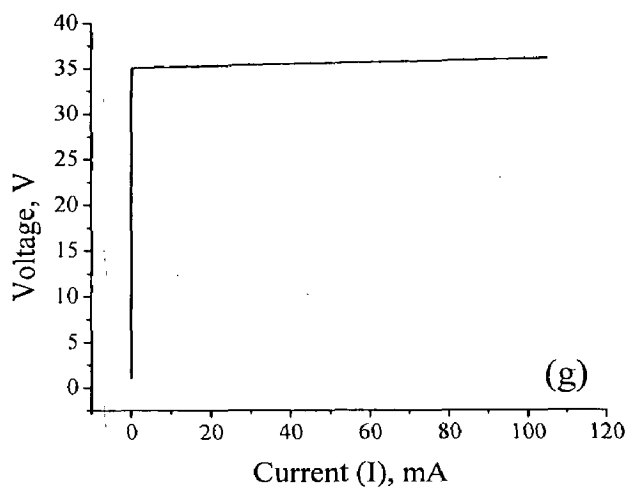3. No significant difference in the quality and the electrical performance of the thin films synthesized either by using pre-synthesized ZnO doped powder dispersed sol or using precursor sol. Therefore the powder dispersed sol was not used for further preparation of the films.

4. Multilayer films prepared by pyrolysis at 240°C after every layer of deposition show strong and clear peaks in XRD patterns.

5. The minority secondary phases $Zn_3(VO_4)_2$ and $Zn_4V_2O_9$ were detected from the samples annealed at 700°C. These secondary phases are found in the bulk varistor samples when sintered at 900°C.

6. FESEM micrographs show that the film prepared is uniform and the grain sizes are in the range of 25-40 nm and 70-90 nm for doped ZnO films annealed at 550°C and 700°C respectively.

7. The α values are higher for the doped samples compared to the undoped samples.

8. The samples annealed at 700°C have higher α values and lower breakdown voltage than that of the samples annealed at 550°C.

7. SUGGESTIONS FOR FUTURE WORK

The following suggestions are put forward for the future work:

1. In the present study three different doping concentrations of 0.5, 1.0 and 1.5 mol% MnO in ZnO-0.5mol%V_2O_5 system have been considered. One can further consider other doping levels to study the effect of doping concentration on micro-structural morphology and the distribution of phases that develop in the sintered samples.

2. A relation could be established between the doping levels and values of non linear coefficient.

3. Further, studies can also be conducted to observe the effect of varying film thickness on the non ohmic behaviour of the ceramic film.

4. Most of the studies for V-I characteristics have been conducted at room temperature. So there is no thermal stress acting on the film. This leaves a large scope for studies to be conducted to analyse the effect of thermal stress on the non ohmic behaviour of films, by doing V-I characterization at higher temperatures.

5. Further, studies can be conducted for optimization of grain size in the film produced by varying the film deposition and annealing parameters and the effect of the same on micro-structural morphology as well as the electrical behaviour can be analysed.

6. Capacitance vs. voltage characteristics of the thin film samples can be studied and therefrom density of states at the grain boundary interfaces can be estimated.

7. Degradation behaviour of the thin film varistor samples can be investigated.

REFERENCES

1. Michio Matsuoka, *"Non-ohmic behaviour of ZnO ceramics"*, Japanese Journal of Applied Physics, 1971, 10 (6), 736-746

2. Takeshi Ito, Shuzo Harried, Michael C. Scott, Carlos A. Paz de Marajo, Larry D. McMillan, *"ZnO thin films and method of making the same"*, United States Patent 5699035, 1997

3. Slavko Bernik, Sreco Macek, Ai Bui, *"The characteristics of ZnO-Bi$_2$O$_3$ based varistor ceramics doped with Y$_2$O$_3$ and varying amounts of Sb$_2$O$_3$"*, Journal of European Ceramic Society, 2004, 24, 1195-1198

4. Neil J. Kinder, Nicola H. Perry, T. O. Mason, Edward J. Garboczi, *"The brick layer model revisited: Introducing the Nano Grain Composite model"*, Journal of American Ceramic Society, 2008, 91 (6), 1733-1746

5. Kazuo Eda, *"Zinc oxide varistors"*, IEEE Electrical Insulation Magazine, November/December 1989, 5 (6), 28-41

6. C.-W. Nahm, *"Effect of MnO2 addition on microstructure and electrical properties of ZnO–V2O5-based varistor ceramics"*, Ceramics International, 2009, 35, 541-546

7. Levinson, L. M. and Philipp, H. R., *"Zinc oxide varistors—A review"*, Journal of American Ceramic Society, 1986, 65, 639-646

8. Gupta, T. K., *"Application of zinc oxide varistors"*, Journal of American Ceramic Society, 1990, 73, 1817-1840

9. Clarke, D. R., *"Varistor ceramics"*, Journal of American Ceramic Society, 1999, 82, 485-502.

10. Mantas, P. Q. and Baptista, J. L., *"The barrier height formation in ZnO varistor"*, Journal of European Ceramic Society, 1995, 15, 605-615

11. Kuo, C. T., Chen, C. S. and Lin, I. N., *"Microstructure and nonlinear properties of microwave-sintered ZnO–V₂O₅ varistors: II, Effect of Mn₃O₄ doping"*, Journal of American Ceramic Society, 1998, 81, 2949-2956

12. Hng, H. H. and Knowles, K. M., *"Microstructure and current– voltage characteristics of multicomponent vanadium-doped zinc oxide varistors"*, Journal of American Ceramic Society, 2000, 83, 2455-2462.

13. Hng, H. H. and Chan, P. L., *"Effects of MnO₂ doping in V₂O₅-doped ZnO varistor system"*, Materials Chemistry and Physics, 2002, 75, 61-66.

14. Heriberto Pfeiffer, Kevin M. Knowles, *"Effects of vanadium and manganese concentrations on the composition, structure and electrical properties of ZnO-rich MnO₂–V₂O₅–ZnO varistors"*, Journal of the European Ceramic Society, 2004, 24, 1199-1203

15. C-W. Nahm, *"Microstructure and varistor properties of ZnO–V₂O₅–MnO₂-based ceramics"*, Journal of Materials Science, 2007, 42, 8370-8373

16. Z. Banu Bahs_i, A. Yavuz Oral, *"Effects of Mn and Cu doping on the microstructures and optical properties of sol–gel derived ZnO thin films"*, Optical Materials, 2007, 29, 672-678

17. Jyh-Kuang Tsai, Tai-Bor Wu, *"Microstructure and nonohmic properties of binary ZnO-V₂O₅ ceramics sintered at 900°C"*, Materials Letters, 1996, 26, 199-203

18. C.T. Kuo, C.S. Chen, I.-N. Lin, *"Microstructure and nonlinear properties of microwave-sintered ZnO-V₂O₅ varistors: I, effect of V₂O₅ doping"*, Journal of American Ceramic Society, 1998, 81, 2942-2948

19. Hui Lu, Yuele Wang, Xian Lin, *"Structures, varistor properties, and electrical stability of ZnO thin films"*, Materials Letters, 2009, 63, 2321-2323

20. Zhifeng Liu, Zhengguo Jin, Wei Li, Jijun Qiu, *"Preparation of ZnO porous thin films by sol gel method using PEG template"*, Materials Letters, 2005, 59, 3620 - 3625

21. Sheng-Yuan Chu, Tser-Min Yan, Shen-Li Chen. *"Analysis of ZnO varistors prepared by the sol-gel method"*, Ceramics International, 2000, 26, 733-737

22. Y. Natsume, H. Sakata, *"Zinc oxide films prepared by sol-gel spin-coating"*, Thin Solid Films, 2000, 372, 30-36

23. Yanqiu Q. Huang, Liu Meidong, Zeng Yike, Li Churong, Xia Donglin, Liu Shaobo, *"Preparation and properties of ZnO-based ceramic films for low-voltage varistors by novel sol-gel process"*, Materials Science and Engineering, 2001, B86, 232-236

24. R. W. Jones, *"Fundamental Principles of Sol-Gel Technology"*, The. Institute of Metals, London, 1989

25. C. J. Brinker and G. W. Scherer, *"Sol-Gel Science : The Physics and Chemistry of Sol-Gel Processing"*, Academic Press, London, 1990, 48-58

26. C. J. Brinker, B. C. Bunker et al., *"Structure of Sol-Gel Derived Inorganic Polymers: Silicates and Borates"*, Journal of the American Chemical Society, part II, 1988, 360, 26, 314-332

27. Gregory A. Luurtsema, *"Spin coating for rectangular substrates"*, The department of electrical engineering and computer sciences, University of California, Berkeley, July 11, 1997

28. Carcano, G.; Ceriani, M.; and Soglio, F. *"Spin Coating with High Viscosity Photoresist on Square Substrate"*, Journal of Microelectronics International, 1993, 10 (3), 12 - 20
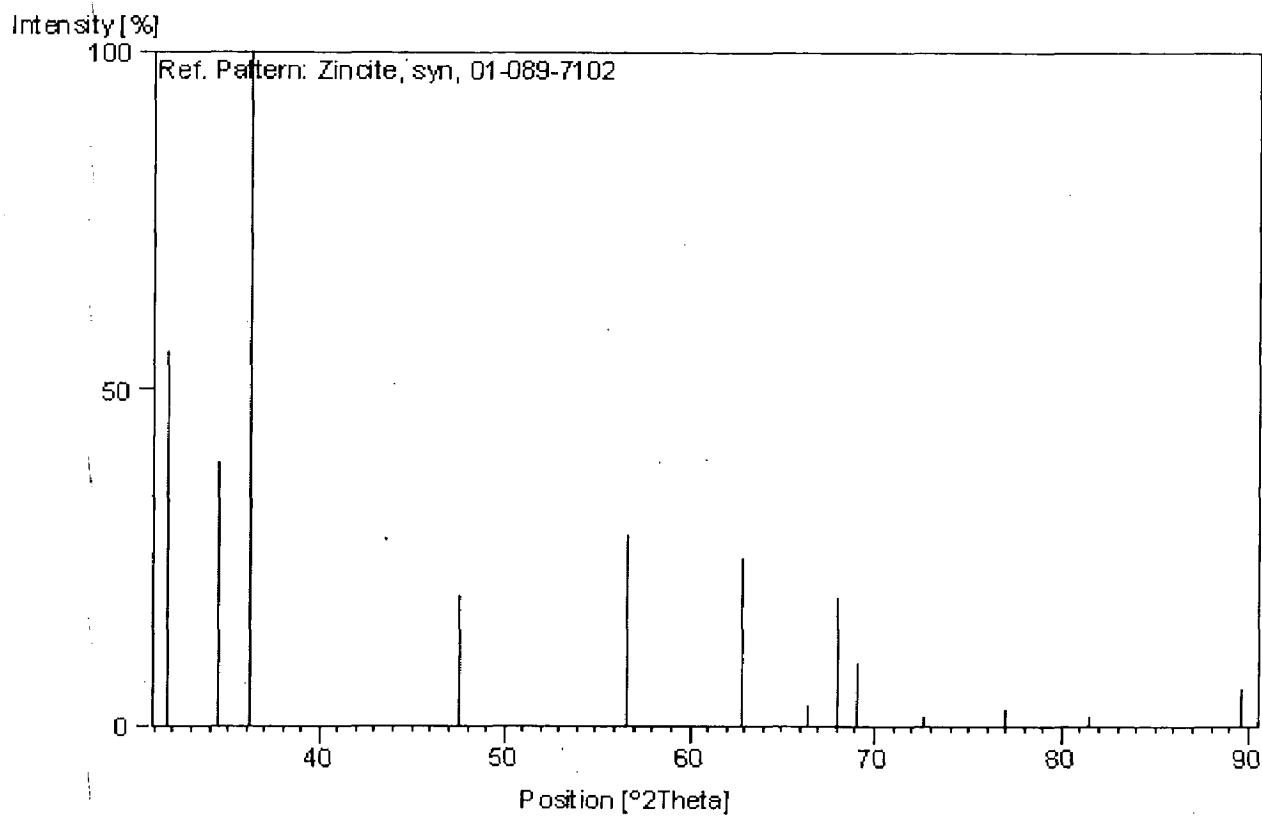
APPENDIX

A1: JCPDS reference file for ZnO

Reference code: 01-089-7102

ICSD name: Zinc Oxide
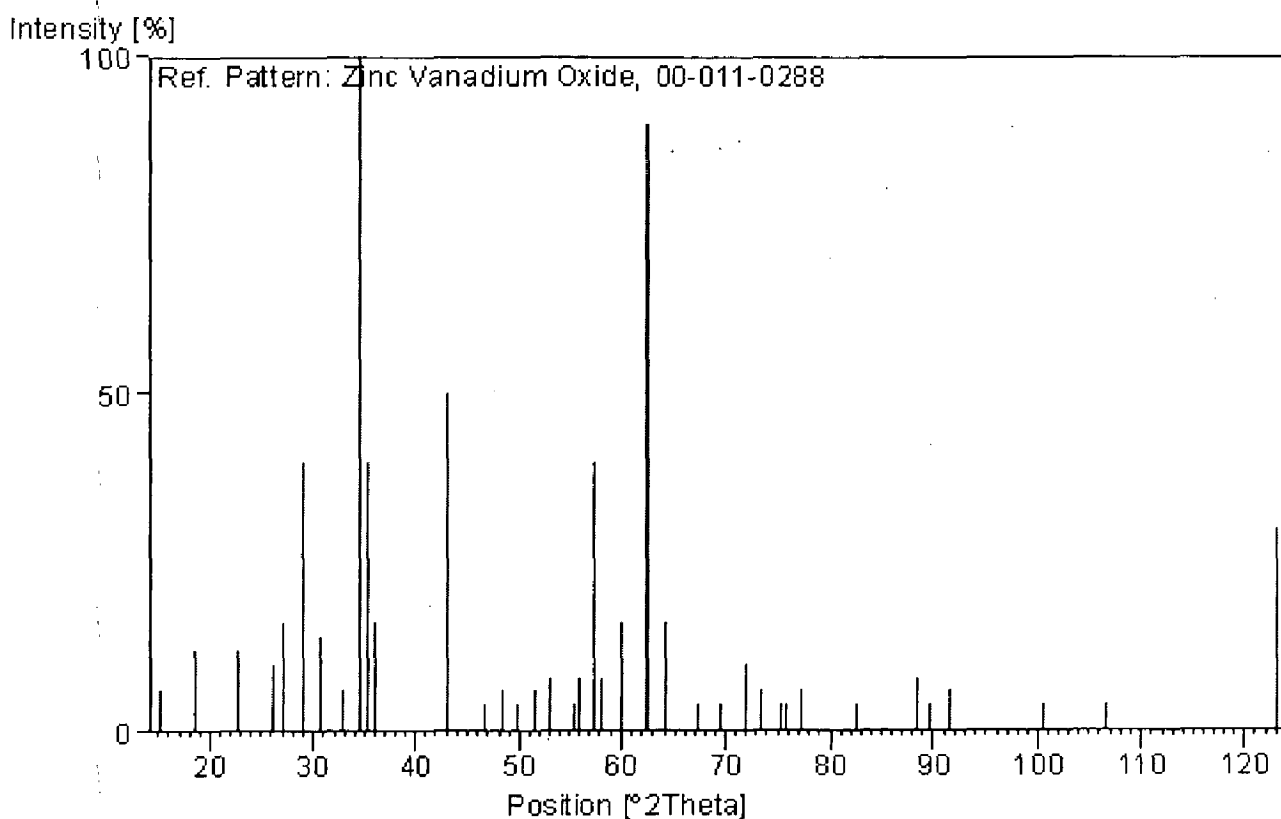
Chemical formula: ZnO

Ref. Pattern: Zincite, syn, 01-089-7102

A2: JCPDS reference file for Zn₃(VO₄)₂

Reference code: 00-011-0288

PDF index name: Zinc Vanadium Oxide

Chemical formula: $Zn_3(VO_4)_2$
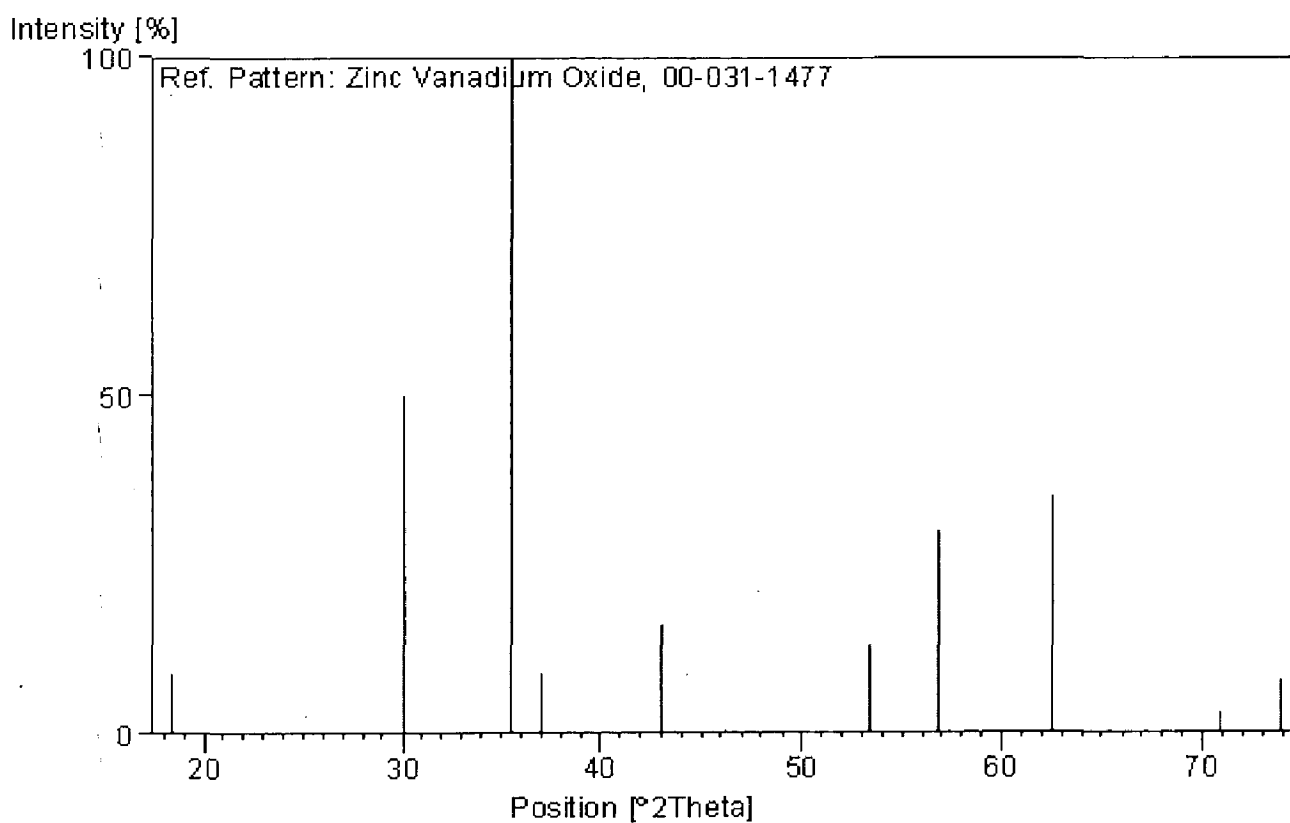
A3: JCPDS reference file for $Zn_3V_3O_8$

Reference code:	00-031-1477
PDF index name:	Zinc Vanadium Oxide
Chemical formula:	$Zn_3V_3O_8$

Intensity [%]

Ref. Pattern: Zinc Vanadium Oxide, 00-031-1477

Position [°2Theta]

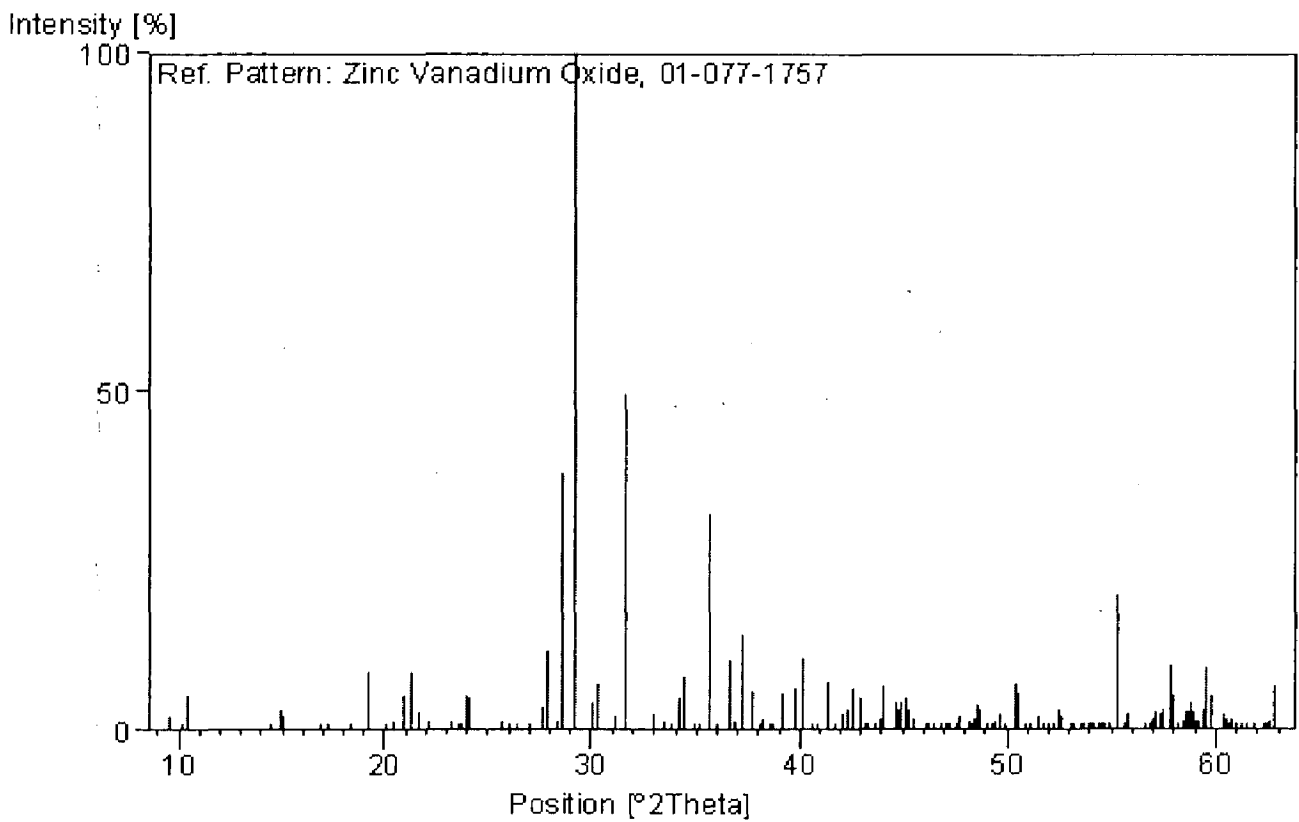## A4: JCPDS reference file for $Zn_4V_2O_9$

Reference code: 01-077-1757

ICSD name: Zinc Vanadium Oxide

Chemical formula: $Zn_4V_2O_9$

A5: JCPDS reference file for ZnV_2O_4

Reference code:	01-075-0318
ICSD name:	Zinc Vanadium Oxide
Chemical formula:	ZnV_2O_4

Intensity [%]

Ref. Pattern: Zinc Vanadium Oxide, 01-075-0318

Position [°2Theta]
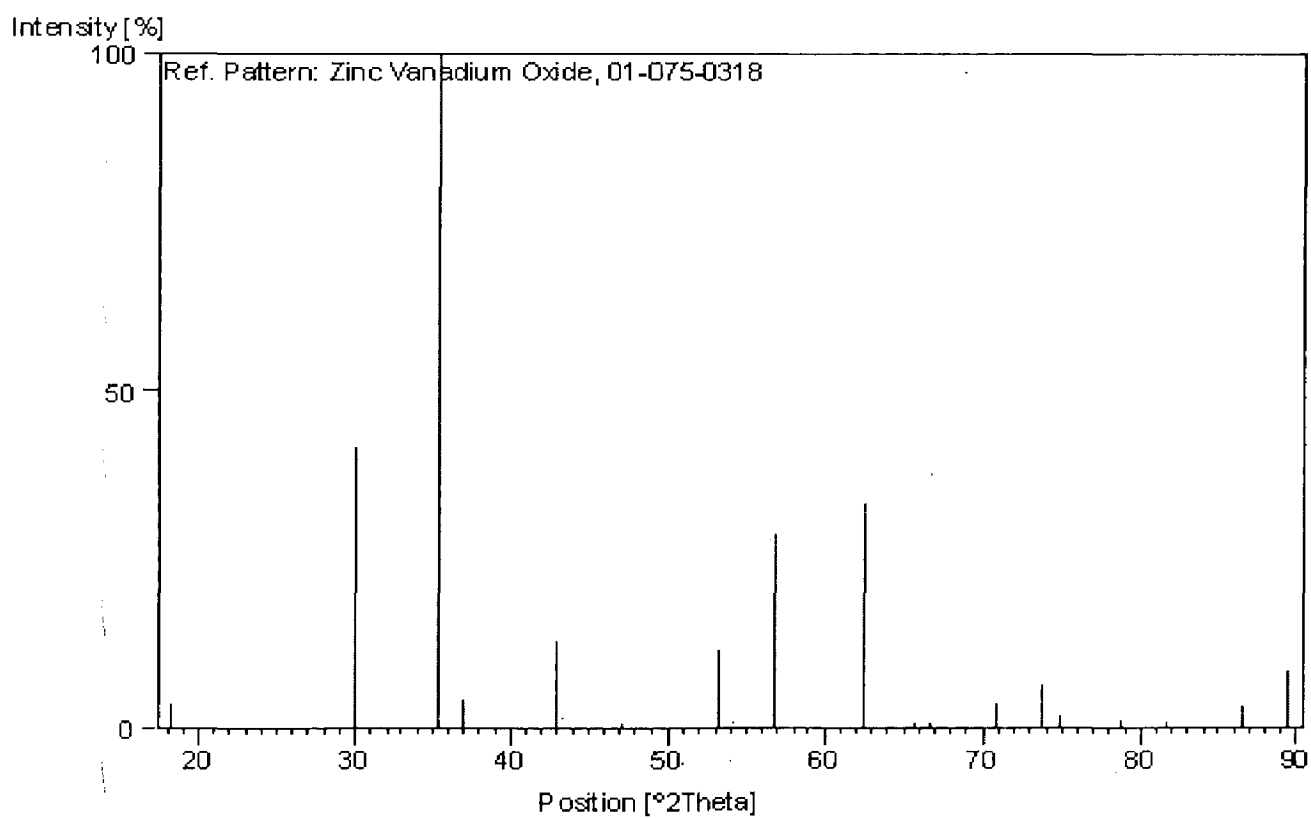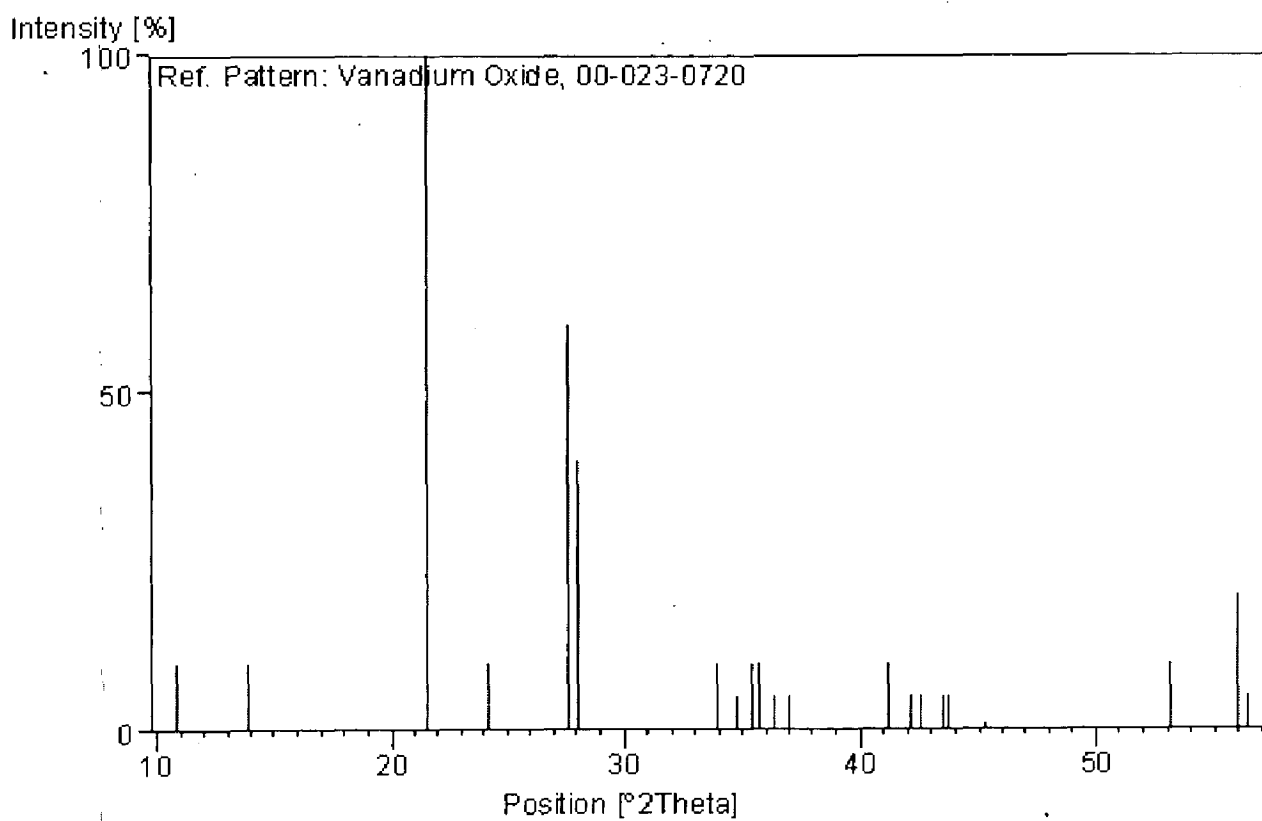
A6: JCPDS reference file for V_4O_9

Reference code: 00-023-0720

PDF index name: Vanadium Oxide

Chemical formula: V_4O_9
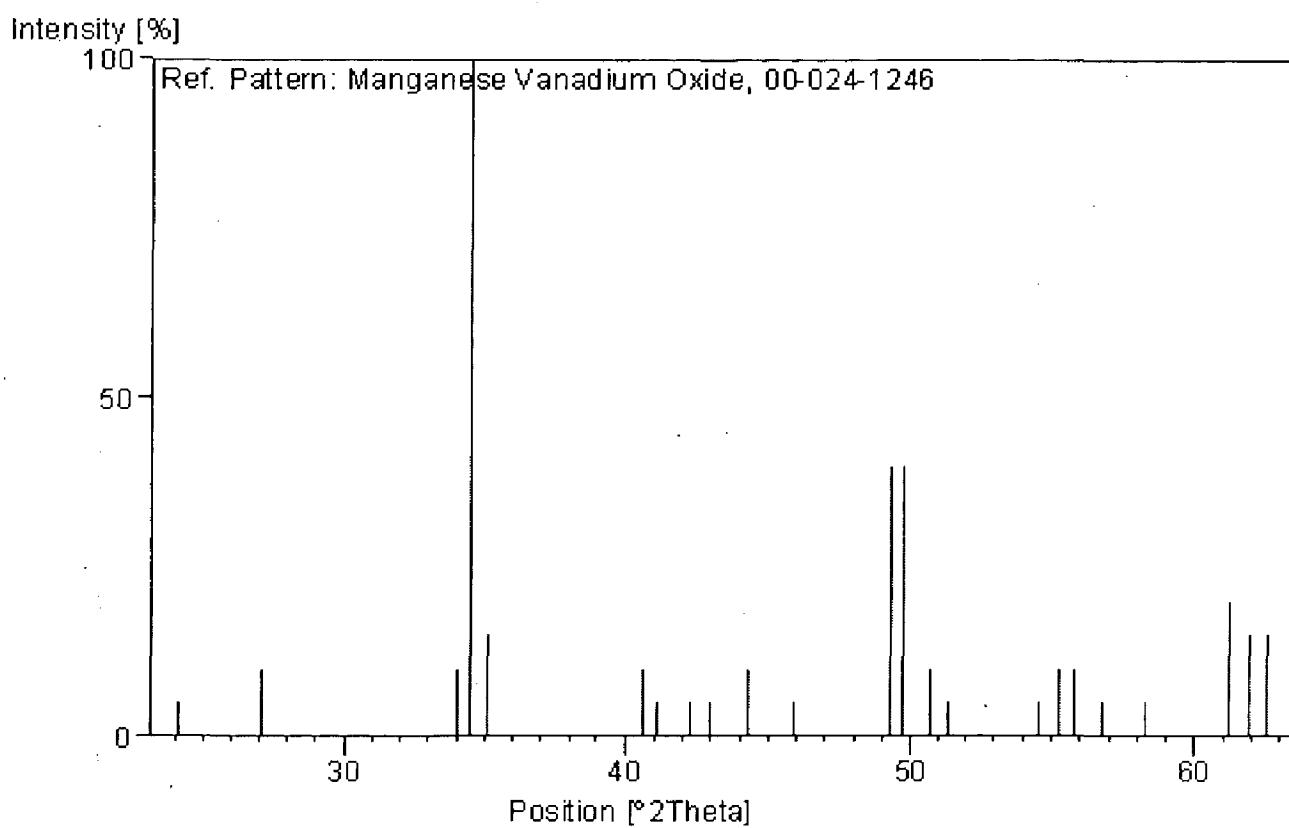

Ref. Pattern: Vanadium Oxide, 00-023-0720

A7: JCPDS reference file for MnVO₃

Reference code: 00-024-1246

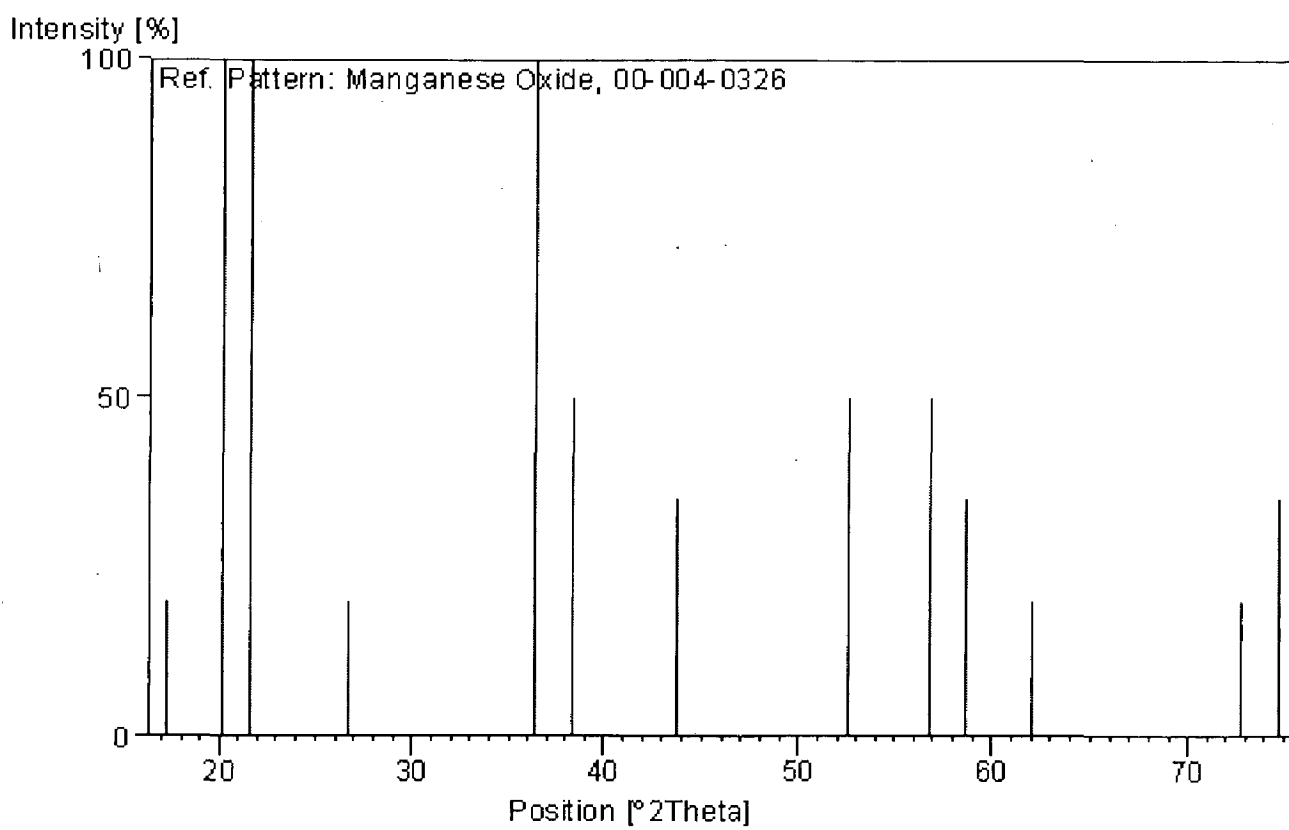PDF index name: Manganese Vanadium Oxide

Chemical formula: MnVO₃

Intensity [%]

Ref. Pattern: Manganese Vanadium Oxide, 00-024-1246

Position [°2Theta]

A8: JCPDS reference file for MnO

Reference code: 00-004-0326

PDF index name: Manganese Oxide

Chemical formula: MnO

Intensity [%]

Ref. Pattern: Manganese Oxide, 00-004-0326

Position [°2Theta]

A9: JCPDS reference file for MnO$_2$

Reference code: 00-044-0141

PDF index name: Manganese Oxide

Chemical formula: MnO$_2$

Ref. Pattern: Manganese Oxide, 00-044-0141